

¹ Inhibition drives habituation of a larval zebrafish visual response

³ Laurie-Anne Lamiré¹, Martin Haesemeyer², Florian Engert^{3,4†},

⁴ Michael Granato^{5†}, Owen Randlett^{1†,*}

*Correspondence:

owen.randlett@
univ-lyon1.fr (OR)

[†]Equal
contribution

⁵ Laboratoire MeLiS, UCBL - CNRS UMR52684 - Inserm U1314, Institut NeuroMyoGène, Faculté de Médecine et de Pharmacie, 8 avenue Rockefeller, 69008, Lyon, France ; ⁶ The Ohio State University, Department of Neuroscience, Columbus, OH 43210, USA ; ⁷ Department of Molecular and Cellular Biology, Faculty of Arts and Sciences, Harvard University, Cambridge, MA 02138, USA ; ⁸ Center for Brain Science, Faculty of Arts and Sciences, Harvard University, Cambridge, MA 02138, USA ; ⁹ Department of Cell and Developmental Biology, University of Pennsylvania, Perelman School of Medicine, 421 Curie Blvd, Philadelphia, PA 19104, USA

10

Abstract Habituation allows animals to learn to ignore persistent but inconsequential stimuli. Despite being the most basic form of learning, a consensus model on the underlying mechanisms has yet to emerge. To probe relevant mechanisms we took advantage of a visual habituation paradigm in larval zebrafish, where larvae reduce their reactions to abrupt global dimming (a dark flash). Using Ca^{2+} imaging during repeated dark flashes, we identified 12 functional classes of neurons that differ based on their rate of adaptation, stimulus response shape, and anatomical location. While most classes of neurons depressed their responses to repeated stimuli, we identified populations that did not adapt, or that potentiated their response. To identify molecular players, we used a small molecule-screening approach to search for compounds that alter habituation learning. Among the pathways we identified were Melatonin and Estrogen signaling, as well as GABAergic inhibition. By analyzing which functional classes of neurons are GABAergic, and the result of pharmacological manipulations of the circuit, we propose that GABAergic inhibitory motifs drive habituation, perhaps through the potentiation of GABAergic synapses. Our results have identified multiple molecular pathways and cell types underlying a form of long-term plasticity in a vertebrate brain, and allow us to propose the first iteration of a model for how and where this learning process occurs.

25

26 Introduction

27 A central function of the brain is to learn and change with experience. These adaptations can reflect attempts to
28 identify and attend preferentially to salient stimuli. For example, identifying the smell of a predator or prey may be
29 crucial, while identifying that my home still smells like my kin is not. This ability to suppress responses to continuous
30 non-salient stimuli is known as habituation, a process generally considered to be the simplest form of learning and
31 memory (*Rankin et al., 2009*). Habituation is conserved across all animals, and like other forms of plasticity, exists in
32 at least two mechanistically distinct forms: transient short-term habituation, and protein-synthesis dependent long-
33 term habituation. Here we focus on long-term habituation, which serves as a pragmatic model to dissect plasticity
34 processes in neural circuits.

35 Work on long-term habituation in various species and paradigms has led to significant insights into the adap-
36 tions underlying this process (*Cooke and Ramaswami, 2020; McDiarmid et al., 2019b*), nonetheless a consensus
37 model on the general principles underlying habituation is yet to emerge. Physiological and genetic work in *Aplysia*,
38 and *C. elegans* were consistent with a model in which homosynaptic depression of excitatory synapses drives habit-
39 uation (*Bailey and Chen, 1983; Rose et al., 2003*) (although see (*Glanzman, 2009*)). In contrast, work in the *Drosophila*
40 olfactory and gustatory systems indicate that the potentiation of inhibitory neurons drives habituation rather than
41 depression of excitatory connections (*Das et al., 2011; Paranjpe et al., 2012; Trisal et al., 2022*), and habituation to
42 specific orientations of visual cues in mice is associated with the potentiation of neuronal activity and synapses in the

43 visual cortex (*Cooke et al., 2015*), which requires GABAergic interneurons (*Kaplan et al., 2016; Hayden et al., 2021*).
44 These studies are more consistent with a model in which the potentiation of inhibition, rather than depression of
45 excitation, drives habituation (*Cooke and Ramaswami, 2020*).

46 Recently, we found that long-term habituation of the response of larval zebrafish to sudden pulses of whole-field
47 darkness, or dark flashes (DFs), involves multiple molecularly independent plasticity processes that act to suppress
48 different components of the behavioural response (*Randlett et al., 2019*). Similar behavioural, pharmacological, and
49 genetic experiments have led to comparable conclusions in acoustic short-term habituation (*Nelson et al., 2022*),
50 and habituation in *C. elegans* (*McDiarmid et al., 2019a,b*), indicating that habituation generally acts via multiple
51 modular plasticity processes. These modules act to mute or shift behavioural responses to repeated stimuli. How
52 and where these processes are implemented in the circuit, and how conserved or derived these processes are across
53 species or paradigms remains to be determined. Here we have used a combination of high-throughput behavioural
54 analyses, pharmacology and whole brain imaging to dissect DF habituation, arriving at a model where GABAergic
55 inhibition drives habituation and suppresses behavioural output.

56 Results

57 Volumetric 2-photon Ca²⁺ imaging of habituation learning

58 When stimulated with a dark flash (DF), larval zebrafish execute an O-bend response (*Figure 1A*). The O-bend is char-
59 acterised by a strong body bend and a large turn that forms part of the phototactic strategy of larval zebrafish, help-
60 ing them navigate towards lit environments (*Burgess and Granato, 2007; Chen and Engert, 2014*). When presented
61 with repeated DFs, larvae habituate and reduce their responsiveness, remaining hypo-responsive for multiple hours
62 (*Figure 1B*), (*Randlett et al., 2019*).

63 To explore the circuit mechanisms leading to this form of habituation, we asked how individual neurons within
64 the DF responsive circuit adapt to repeated dark flashes. We used a head-fixed paradigm to perform 2-photon Ca²⁺
65 imaging in larvae expressing nuclear-targeted GCaMP7f pan-neuronally. Imaging was performed with a resonant
66 scanner and piezo objective, enabling us to cover a volume of $\approx 600 \times 300 \times 120 \mu\text{m}$ (x,y,z) sampled at $0.6 \times 0.6 \times 10$
67 μm resolution, leading to the detection of 30890 ± 3235 ROIs per larvae ($\pm\text{SD}$, *Figure 1C-E*). ROIs were aligned to the
68 Z-Brain atlas coordinates (*Randlett et al., 2015*), demonstrating that this volume spans the majority of the midbrain,
69 hindbrain, pretectum and thalamus (*Figure 1C-E*).

70 We focused on a single training block of 60 DFs, as this is the period during which the strongest learning takes
71 place (*Figure 1Bi*). This paradigm induced strong Ca²⁺ activity in neurons (*Figure 1F*), some of which were clearly
72 associated with the DF stimuli. Ca²⁺ transients in response to DFs generally decreased across the 60 stimuli, though
73 this pattern was not seen in all neurons, and substantial heterogeneity in their adaptations were observed. Strong
74 correlated patterns were also seen in large groupings of neurons, predominantly in the hindbrain, which were
75 associated with movement events through their correlation with motion artifacts in the imaging data (*Figure 1-figure
76 Supplement 1*).

77 To explore the spatial patterns in these data we used a 2-dimensional lookup table to visualize tuning with regres-
78 sors representing either DF stimuli or movement (*Figure 1G, H*). This revealed segregated populations of neurons
79 coding for the DFs (pink) and movement (green/teal). As expected, DF-tuned neurons were located predominantly
80 in visual sensory areas of the midbrain (tectum) and the diencephalon (pretectum and thalamus). Motor-coding neu-
81 rons dominated in the hindbrain, with the exception of the cerebellum and inferior olive, which was predominantly
82 tuned to the sensory stimulus. Some neurons did show approximately equal correlation values to both stimuli, as
83 evidenced by the blue-ish hues. Finally, some areas of the brain appeared to contain mixtures of neurons with
84 different coding properties, including the ventral diencephalon and midbrain.

85 To determine if there was any spatial logic to how different neurons adapt their responsiveness to DFs during
86 imaging, we plotted the ROIs using a lookup table highlighting the preference of for either the first three DFs (pink,
87 naive response), or last three DFs (green, trained response). Strong preferences for the naive stimuli reflects a
88 depressing response profile (*Figure 1I, J*). While most neurons did show tuning consistent with strong depression,
89 there were neurons that showed an equal preference for naive and trained stimuli, or even stronger preference for
90 the latter, indicating stable or potentiating response profiles. These non-depressing neurons were mostly contained

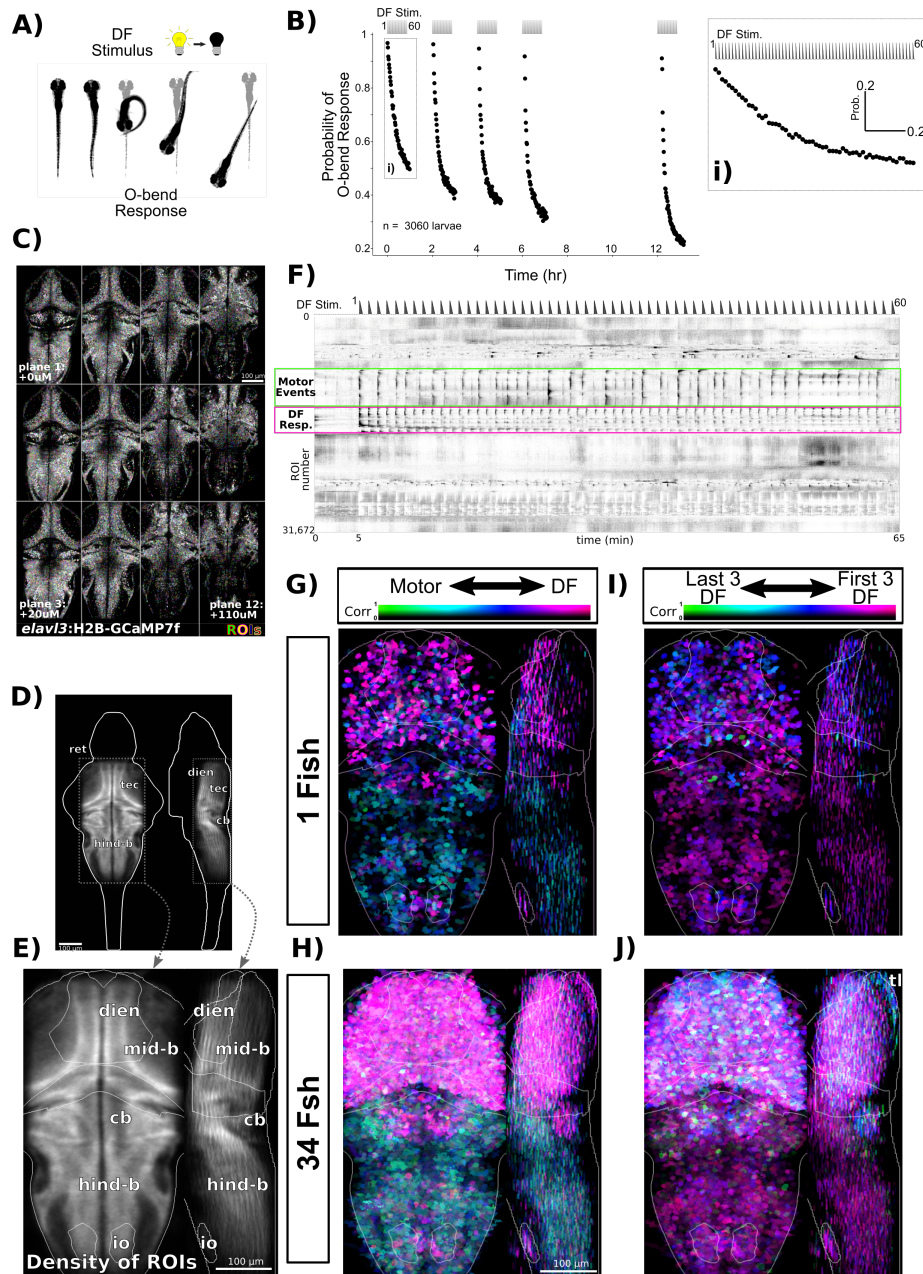


Figure 1. Volumetric 2-photon Ca^{2+} imaging of dark flash habituation.

A) In response to a dark flash (DF), larval zebrafish execute a high-amplitude turn called an O-bend response.

B) Habituation results in a progressive decrease in response probability to dark flashes repeated at 1-minute intervals, delivered in 4 blocks of 60 stimuli, separated by 1hr of rest (from 0:00-7:00), and after a 5hr retention period (12:00-). Inset **i**) shows expanded view of the first training block.

C) *Tg(elavl3:H2B-GCaMP7f)* larvae were imaged across 12 z-planes at $10\mu\text{m}$ steps. ROIs are overlaid in random colors.

D) Density of detected ROIs registered and plotted in the Z-Brain coordinate space. $n=1,050,273$ ROIs across 34 larvae.

E) Cropped field of view used for plotting and analyzing Ca^{2+} imaging data and approximate anatomical localizations of major brain areas: dien=diencephalon, mid-b = midbrain, cb = cerebellum, hind-b = hindbrain, io = inferior olive, ret = retina, tec = tectum

F) Functional responses of neurons to 60 dark flashes at 1-minute intervals, plotted as a clustered heatmap ("rastermap" ([Pachitariu et al., 2017](#), github.com/MouseLand/rastermap)), where rows represent individual neurons ordered by the similarities in their activity. Darker shades reflect increased activity. This clustering reveals neurons that are tuned to the DF stimulus (pink box) or motor events (green box). Dashed trace above the heatmap depicts the DF stimulus convolved with a kernel approximating H2B-GCaMP7f kinetics.

G) ROIs in an individual fish plotted based on their correlation and tuning to regressors defining either Motor or DF stimulus events, highlighting the spatial distributions of these tunings across the imaged population. Plotted as a maximum intensity projection.

H) Same analysis as G, but across the entire population of 34 larvae.

I) ROIs in an individual fish plotted based on their correlation and tuning to regressors defining either the first or last three DF stimuli.

J) Same analysis as I, but across the entire population of 34 larvae. tl = torus longitudinalis

Figure 1—figure supplement 1. Validation of motion analysis based on image artifacts during 2-photon imaging

91 in the dorsal regions of the brain, including the torus longitudinalis, cerebellum and dorsal hindbrain. These results
92 demonstrate that while the majority of neurons across the brain depress their responsiveness during habituation,
93 a smaller population of neurons exists that show the opposite pattern.

94 These results indicate that habituation does not occur via a simple excitatory bottleneck in the sensory system,
95 as in such a model neurons that show stable responses or that potentiate would not be observed in downstream
96 regions. The fact that non-depressing neurons are observed within the hindbrain demonstrates that motor-related
97 brain regions contain non-depressed signals, and therefore likely contribute to habituation plasticity.

98 **Functional classification and anatomical localization of neuronal types observed during habitua- 99 tion learning**

100 To explore the functional heterogeneity within the DF-tuned neurons we used affinity propagation clustering. This
101 method has the advantage that cluster numbers do not need to be defined beforehand, and instead attempts to
102 identify the most representative response profiles (*Förster et al., 2020*). This identified 12 clusters that differed both
103 in their adaptation to repeated DFs, as well as the shape of their response to the DF (*Figure 2A,B*).

104 We therefore use these two aspects of the response to label the clusters:

105 Adaptation Profile

106 **No Adaptation** = noA : Cluster 1, 9, 10

107 **Weak Depression** = weakD : Cluster 5, 6, 11

108 **Medium Depression** = medD : Cluster 2, 3, 7

109 **Strong Depression** = strgD : Cluster 4, 8

110 **Potentiation** = Pot : Cluster 12

111 Response Shape

112 **On-response** = $_{On}$: Cluster 1, 2

113 **Long/sustained response** = $_{L}$: Cluster 3, 4

114 **Medium-length response** = $_{M}$: Cluster 5, 6, 9

115 **Short/transient response** = $_{S}$: Cluster 7, 8, 10, 11

116 Yielding clusters: $1_{On}^{noA}, 2_{On}^{medD}, 3_L^{medD}, 4_L^{strgD}, 5_M^{weakD}, 6_M^{weakD}, 7_S^{medD}, 8_S^{strgD}, 9_M^{noA}, 10_S^{noA}, 11_S^{weakD},$ and 12_M^{Pot}

117 While these results indicate the presence of a dozen functionally distinct neuron types, such clustering analyses will
118 force categories upon the data irrespective of if such categories actually exist. To determine if our cluster analyses
119 identified genuine neuron types, we analyzed their anatomical localization (*Figure 2C-E*). Since our clustering was
120 based purely on functional responses, we reasoned that anatomical segregation of these clusters would be con-
121 sistent with the presence of truly distinct types of neurons. Indeed, we observed considerable heterogeneity both
122 within and across brain regions. For example: 11_S^{weakD} was mostly restricted to medial positions within the optic
123 tectum; 3_L^{medD} and 4_L^{strgD} were more prevalent within motor-related regions of the brain including the tegmentum
124 and hindbrain rhombomeres; 9_M^{noA} was the most prominent cluster in the torus longitudinalis, consistent with the
125 presence of non-depressing signals in the area (*Figure 1I,J*).

126 We then quantified the similarity in the spatial relationships among the clusters by looking at the correlations in
127 the positions of the ROIs in the Z-Brain (*Figure 2E*). This revealed similar hierarchical relationships to those identified
128 functionally (*Figure 2B*), especially with respect to *Response Shape*, indicating that physical location is associated with
129 functional response type.

130 Finally, since our functional analysis was performed purely based on correlations with the DF stimuli, we asked to
131 what extent neurons belonging to each cluster were correlated with motor output (*Figure 2F*). This identified 4_L^{strgD} as
132 the most strongly correlated to motor output, consistent with its strong habituation profile and its localization within
133 motor-regions of the hindbrain. This indicates that 4_L^{strgD} neurons likely occupy the most downstream positions
134 within the sensory-motor network.

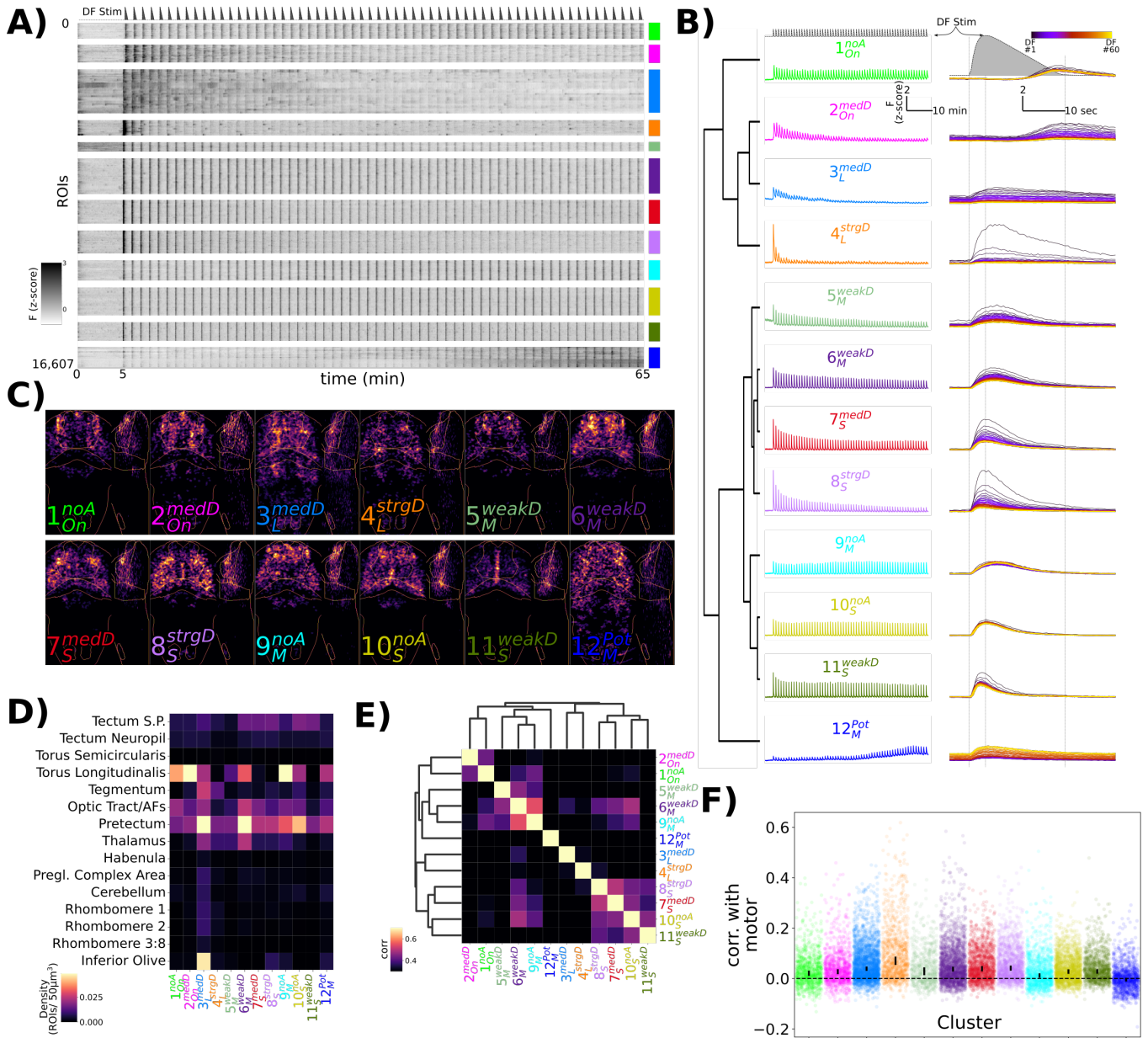


Figure 2. Characterization of functional response types during habituation learning.

A) Heatmap of the response profiles of ROIs categorized into 12 functional clusters. n=16,607 ROIs from 34 larvae.

B) Average z-scored fluorescence of each functional cluster plotted for the whole experiment (left column), and centered on each DF stimulus (right column), demonstrating the differences in both *Adaptation Profiles* and *Response Shape* for each cluster. Clusters were identified using Affinity Propagation clustering (affinity = Pearson correlation, damping = 0.9, preference = -9), and organized using Hierarchical clustering, distance = complete, correlation. Dashed lines in top panels are the DF stimulus convolved with a kernel approximating H2B-GCaMP7f kinetics, used as the regressor in the analysis.

C) Summed intensity projection of the ROIs belonging to each functional cluster in Z-Brain coordinate space depicting their physical locations in the brain. Projection images are normalized to the maximum value.

D) Heatmap depicting the density of each cluster that is found within different Z-Brain regions.

E) Correlogram calculated from the Pearson correlation in downsampled volumes for the ROI centroid positions for each cluster (see Methods). Hierarchical clustering, distance = complete, correlation.

F) Correlation between motor events and the Ca²⁺ traces for each ROI assigned to the functional clusters. dots = individual ROIs, bar height = 99.9999% confidence interval around the median value.

135 These results highlight a diversity of functional neuronal classes active during DF habituation. Whether there
136 are indeed 12 classes of neurons, or if this is an over- or under-estimate, awaits a full molecular characterization.
137 Independent of the precise number of neuronal classes, we proceed under the hypothesis that these clusters define
138 neurons that play distinct roles in the DF response and/or its modulation during habituation learning.

139 **Pharmacological screening to identify habituation modulators**

140 We next used a pharmacological screening approach to both identify molecular mechanisms of habituation and to
141 further probe the habituating circuit. For this we screened 1953 small molecule compounds with known targets
142 (*Figure 3-source data 1*), in conjunction with the high-throughput assay we previously established, which has a
143 maximum throughput of 600 larvae/day (*Figure 3A*, (*Randlett et al., 2019*)). As we aimed to identify modulators
144 specific for habituation, we included additional behavioural assays as controls, including the response to acoustic
145 stimuli, the optomotor response, and the spontaneous swimming behaviour of the fish in the absence of stimulation
146 (*Figure 3B,C*). In each 300-well plate, 40 groups of 6 larvae were treated in individual wells, and compared to 60
147 vehicle treated controls (*Figure 3A*). We chose these numbers based on a sub-sampling analysis that determined
148 these numbers were sufficient to identify the effect of a known modulator of habituation (haloperidol (*Randlett*
149 *et al., 2019*)) at a false-negative rate of less than 0.05 (not shown), while allowing us to screen 80 compounds per
150 experiment across 2 plates.

151 We were able to collect the full behavioural record of 1761 compounds (*Figure 3D*, *Figure 3-source data 2*)),
152 indicating that the fish survived the treatment and maintained their ability to swim. Behavioural records for fish
153 treated with each compound were compressed into a fingerprint (*Rihel et al., 2010*) – a vector representing the
154 strictly standardised mean difference (SSMD) across 47 aspects of behaviour (see Methods). For measurements
155 related to dark-flash habituation behaviour, responses were time-averaged across three epochs chosen to highlight
156 changes in habituation: the naive response (first 5 dark flashes), the response during the remaining training flashes,
157 and the re-test block 5 hrs after training (*Figure 3B*). This was done across 10 different components of the dark flash
158 response (Probability of Response, Latency, Displacement, etc.).

159 We found that 176 compounds significantly altered at least one aspect of measured behaviour, yielding a 9% hit
160 rate (hit threshold of $|SSMD| \geq 2$). While the average effect was to suppress behavioural output ($\overline{SSMD} = -0.20$),
161 which could reflect non-specific toxicity or a generalized inhibition of motor output, most small molecules induced
162 both positive and negative changes in behavioural output, indicating that toxicity is not the primary phenotypic
163 driver. While the false negative rate is difficult to determine since so little is known about the pharmacology of the
164 system, we note that of the three small molecules we previously established to alter dark flash habituation that
165 were included in the screen, Clozapine, Haloperidol and Pimozide (*Randlett et al., 2019*), two were identified among
166 our hits.

167 **Correlational structure in the pharmaco-behavioural space**

168 To explore the pharmaco-behavioural space in our dataset we clustered the hits based on their behavioural phe-
169 notypes (*Figure 4A*). This strategy can identify compounds that share common pharmacological targets, or perhaps
170 distinct pharmacological targets that result in convergent behavioural effects (*Bruni et al., 2016; Rihel et al., 2010*).
171 Indeed, compounds known to target the same molecular pathways often showed similar behavioural fingerprints ly-
172 ing proximal on the linkage tree, indicating that our dataset contains sufficient signal-to-noise to recover consistent
173 pharmaco-behaviour relationships.

174 Alternatively, compounds can be considered as tools to manipulate different aspects of brain function agnostic to
175 their molecular mechanisms. Consequently, using similarities and differences among the induced alterations should
176 uncover molecular and neural linkages among different behavioural outputs. Following this logic, the ability of a
177 compound to co-modify different aspects of behaviour would reflect molecular and/or circuit-level dependencies.
178 For example, visual behaviours that all depend upon photoreceptors should be similarly affected by any compounds
179 that modulate phototransduction in these photoreceptors. We quantified these relationships by calculating the
180 correlated effects on our different behavioural measurements across compounds (*Figure 4B*).

181 Consistent with our previous results highlighting uncorrelated learning across the behavioural components of
182 the O-bend response during habituation (*Randlett et al., 2019*), we found that different aspects of the response

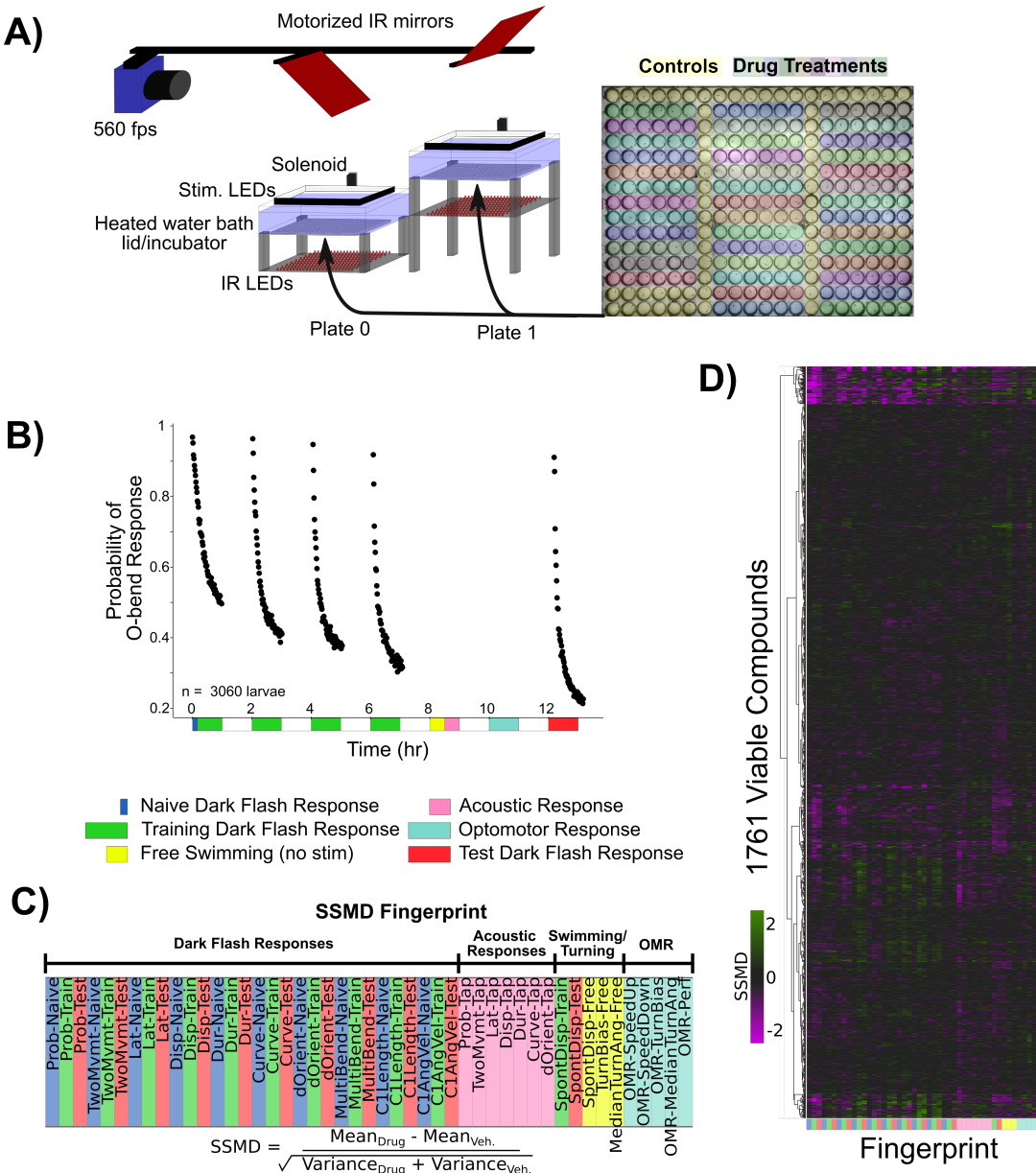


Figure 3. Pharmacological screening for dark flash habituation modulators.

A) Screening setup to record larval zebrafish behaviour in 300-well plates, which are placed below a 31°C water bath that acts as a heated lid for the behaviour plates. Two 300-well plates are imaged in alternation using mirrors mounted on stepper motors. Fish are illuminated with infra-red LEDs and imaged with a high-speed camera recording at 560 frames per second (fps). Visual stimuli are delivered by a rectangular ring of RGB LEDs, and acoustic stimuli are delivered via a solenoid mounted on the back of the water tank. Colors overlaid on the 300-well plate indicate the arrangement of small molecule treatments and controls (yellow).

B) Habituation results in a progressive decrease in responsiveness to dark flashes repeated at 1-minute intervals, delivered in 4 training blocks of 60 stimuli, separated by 1hr of rest (from 0:00-8:00). This epoch is separated into periods reflective of the Naive response (first 5 stimuli, blue), and the remaining 235 stimuli during Training (green). From 8:00-8:30, no stimuli are delivered and fish are monitored for spontaneous behaviour (yellow). From 8:30-9:00 fish are given acoustic stimuli via the solenoid tapping on the water bath (pink). From 10:00 - 11:00 fish are stimulated with alternating leftward and rightward motion using the RGB LEDs to induce the optomotor response and turning towards the direction of motion (light blue). Finally, at 12:00-13:00, larvae are given 60 additional dark flashes during the test period (red).

C) The strictly standardized mean difference (SSMD) is calculated across these different time periods, behaviours and the different components of O-Bend behavioural habituation (Randlett et al., 2019). All compounds were dosed at 10 μ M in 0.1% DMSO ($n = 6$ larvae), relative to 0.1% DMSO vehicle controls ($n = 60$ larvae).

D) These vectors are assembled across all screened compounds that were viable and did not cause death or paralysis of the larvae. Displayed as a hierarchically clustered heatmap of behavioural Fingerprints (vectors of SSMD values). Clustering distance = ward, standardized euclidean.

Figure 3—source data 1. Small molecule library, Selleckchem Bioactive: FDA-approved/FDA-like small molecules

Figure 3—source data 2. Behavioural fingerprints for viable compounds

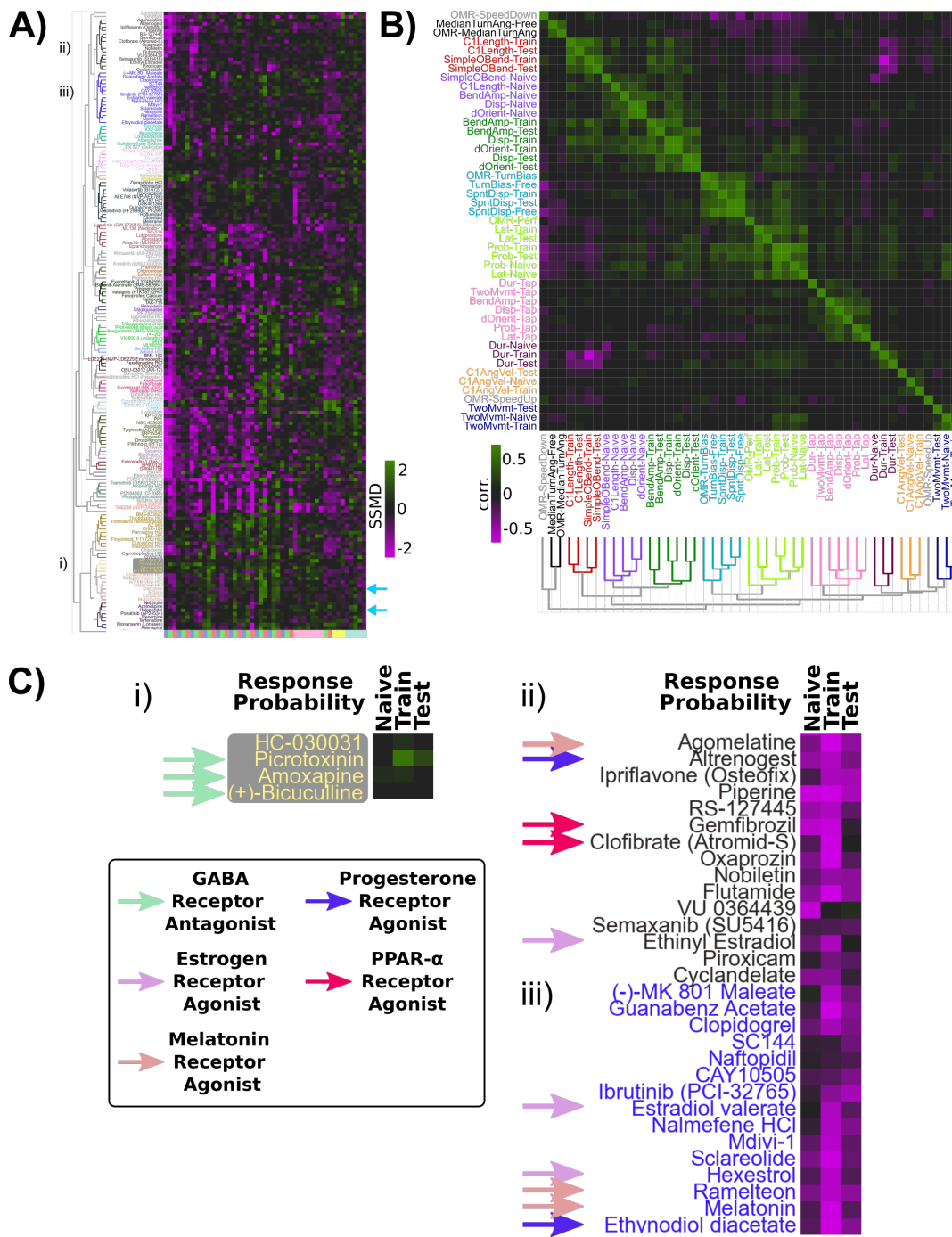


Figure 4. Pharmaco-behavioural analyses of behaviour-modifying compounds.

A) Clustered heatmap of the behavioural Fingerprints for the 176 hits of the screen, showing at least one behaviour measure with $|SSMD| \geq 2$. Clustering distance = ward, standardized euclidean, colour/cluster threshold = 9.5. This led to the re-identification of Haloperidol and Clozapine as habituation modifiers (light blue arrows).

B) Clustered correlogram of the Pearson correlation coefficients for the different measured components of behaviour across hits (same data as (A)) revealing the independence or co-modulation of behaviours. Clustering distance = average, correlation, colour/cluster threshold = 1.5.

C) Subsets of clustered heatmap from (A), highlighting the similar phenotypes exhibited by i) GABA Receptor antagonists and ii), iii) Melatonin receptor agonists, Estrogen receptor agonists, Progesterone receptor agonists and peroxisome proliferator-activated receptor alpha (PPAR α) agonists. Heatmap is cropped to the first three columns of (A), depicting the SSMD of response Probability relative to vehicle controls.

were independently affected pharmacologically, resulting in distinctive correlated groupings within the correlogram. While we previously found that O-Bend response Probability and Latency habituate independently in individual fish (Randlett et al., 2019), in our small molecule screen data these appear to be tightly coupled (Figure 4B). The performance of the animals in the OMR assay under different treatments was also associated with O-bend Probability and Latency, suggesting that pharmacological modulation of vision or arousal could drive these correlations within the small molecule screen dataset.

These analyses confirm habituation behaviour manifests from multiple distinct molecular mechanisms that independently modulate different behavioural outputs.

Modulation of habituation by GABA, Melatonin and Estrogen signaling

For the remainder of the analyses we decided to focus on the mechanisms leading to the habituation of response probability, as this is the criterion for which it is easiest to identify the link between neural activity and behavior, providing the best entry point for studying the circuit mechanisms of long-term habituation. To identify the most promising hits, we sought to identify compounds that:

- 1) Have minimal effects on the naive response to DFs, but strong effects during the training and/or memory-retention periods. This would prioritize pathways that affect habituation, rather than simply DF responsiveness.
- 2) Have minimal effects on other aspects of behaviour, in order to exclude compounds that would alter generalized arousal, movement ability/paralysis, or visual impairment. Such compounds would strongly influence DF responsiveness, but likely independently of pathways related to habituation.
- 3) Show similar behavioural effects to other compounds tested that target the same molecular pathway. Such relationships can be used to cross validate, yet we note that our library choice was very broad, and target coverage is non-uniform. Therefore a lack of multiple hits targeting the same pathway should not be taken as strong evidence of a false positive.

This prioritization led to the identification of the GABA_{A/C} Receptor antagonists Bicuculline, Amoxapine, and Picrotoxinin (PTX). PTX treatment had the strongest effects, with increased responsiveness to DFs during the training and test periods, indicative of defects in habituation (Figure 4Ci). Dose-response experiments confirmed a strong effect of PTX on inhibiting the progressive decrease in responsiveness during habituation learning at 1-10 μM doses (Figure 5A). Importantly, like the naive dark-flash response, the probability of responding to an acoustic stimulus and the optomotor response were not inhibited (Figure 5-figure Supplement 1A). While strong GABA_{A/C}R inhibition results in epileptic activity in larval zebrafish, we did not observe evidence of seizure-like behaviour at these doses, consistent with a partial GABA_{A/C}R in our experiments and previous results (Bandara et al., 2020). Therefore, we conclude that partial antagonism of GABA_AR and/or GABA_CR is sufficient to strongly suppress habituation but not generalized behavioural excitability, indicating that GABA plays a very prominent role in habituation. This is consistent with a model in which the potentiation of inhibition actively silences sensory-induced activity during habituation to suppress motor output (Cooke and Ramaswami, 2020; Ramaswami, 2014).

We next turned our attention to the upper portion of the clustered behavioural fingerprint graph (Figure 4A), where strong and relatively specific inhibition of responsiveness during training and testing were observed, indicative of enhanced habituation (Figure 4Cii, iii). Among the hits observed here were multiple agonists of both Melatonin and Estrogen receptors, indicating that hormonal signaling may play a prominent role in habituation. Dose response studies with Melatonin confirmed strong potentiation of habituation (Figure 5B). Melatonin did cause a decrease in spontaneous movement behaviour, consistent with its role in arousal/sleep regulation in zebrafish and other vertebrates (Gandhi et al., 2015; Zhdanova et al., 2001), yet Melatonin did not inhibit the naive response to dark flashes, the responsiveness to acoustic stimuli or OMR performance (Figure 5B, Figure 5-figure Supplement 1B). Melatonin's effect on habituation was also most prominent for the Probability of response, and did not strongly alter habituation for Displacement Figure 5-figure Supplement 1F, indicating it does not cause generalized sedation but modulates specific aspects of behaviour at these doses, including increasing habituation of the Probability of response.

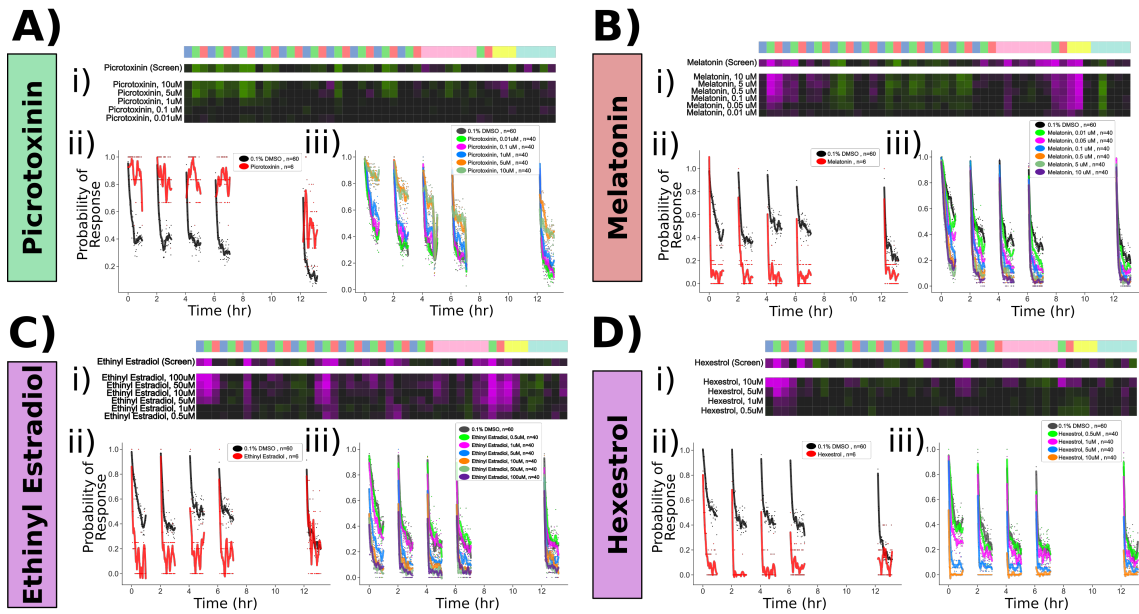


Figure 5. Confirmed pharmacological modulators of habituation.

Dose response studies for **A)** Picrotoxinin, **B)** Melatonin, **C)** Ethynodiol Estradiol and **D)** Hexestrol.

Displayed for each treatment are: i) Behavioural fingerprint for the original screen data (10 μ M), and the dose response data. ii) Original screen data for the probability of response to DF stimuli. Each dot is the probability of response to one flash. Lines are smoothed in time with a Savgolay Filter (window = 15 stimuli, order=2). iii) Dose response data for the probability of response, plotted as in ii)

Figure 5—figure supplement 1. Pharmacological manipulation of control behaviours and response displacement during habituation

We similarly validated that the Estrogen Receptor agonists Ethynodiol Estradiol and Hexestrol, potentiated habituation at 5-100 μ M and 1-10 μ M doses, respectively (**Figure 5C,D**). Ethynodiol Estradiol strongly suppressed movement rates at these doses, and both treatments suppressed acoustic responsiveness and OMR performance at doses $\geq 10 \mu$ M (**Figure 5 - figure Supplement 1C,D**). Thus, it is less clear how specific or generalized Estrogen Receptor agonism is on behaviour, although the effective doses of Hexestrol for influencing habituation (1-5 μ M) were lower than those that significantly affected other behaviours (10 μ M). Nevertheless we decided to focus on PTX and Melatonin for the remaining experiments.

Our screening approach identified both expected (GABA) and unexpected (Melatonin, Estrogen) pathways that strongly modulate habituation of responsiveness. We also implicated other pathways in habituation, including Progesterone and PPAR α (**Figure 4C**), and identified compounds that strongly modify other aspects of behaviour (OMR, acoustic and spontaneous behaviour). These hits can be mined for future projects investigating the molecular basis of behaviour.

Pharmacological manipulations of functional circuit properties during habituation

Our Ca^{2+} imaging experiments identified 12 distinct functional classes of neurons during habituation learning, but it is unclear how these might be organized in a circuit. Based on the diversity of functional response profiles identified, it is clear that solving this circuit will take considerable further work. As a starting point in this long-term effort, we used the pharmacological manipulations as these treatments provide us with tools to ask how treatments that potently alter habituation behaviour also alter the functional properties of neurons. We compared the Ca^{2+} activity patterns after treatment with vehicle (0.1% DMSO), PTX, or Melatonin (**Figure 6**). At the behavioural level, we found a trend indicating that we were able to manipulate habituation pharmacologically in our tethered imaging assay, though this was very subtle (**Figure 6A**). This discrepancy relative to the very strong behavioural effects in freely-swimming animals (**Figure 5**) likely result from the head-restrained protocol, which itself strongly inhibits behavioural output. Yet, since we did observe a trend in behavioural data, we proceeded under the assumption that

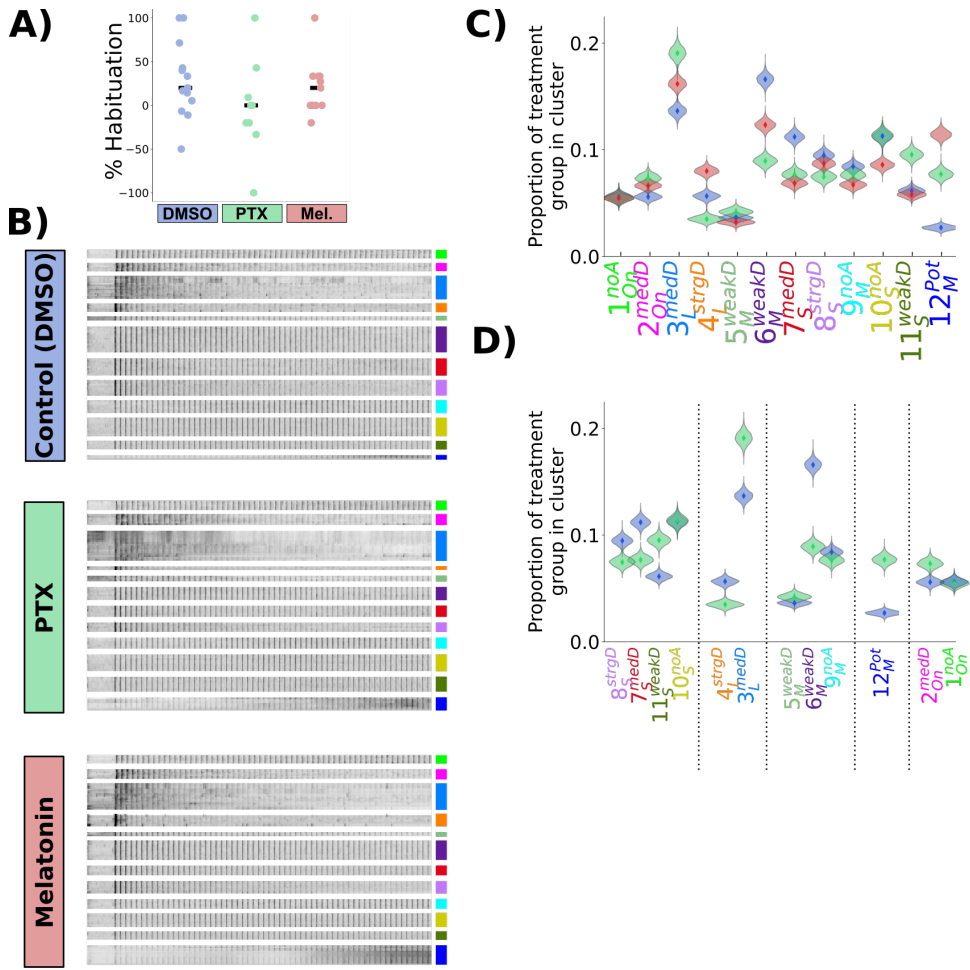


Figure 6. Picrotoxinin and Melatonin alter the proportions of functionally identified neurons
A) Percent habituation for larvae during Ca^{2+} imaging, calculated as: $\% \text{ Habituation} = 100 \times (1 - \frac{P(\text{Resp}_{31 \rightarrow 60})}{0.5 \times (P(\text{Resp}_{1 \rightarrow 30}) + P(\text{Resp}_{31 \rightarrow 60}))})$
B) Heatmap of response profiles of ROIs categorized into the 12 functional clusters from larvae treated with DMSO (vehicle control, n = 428,720 total ROIs in 14 larvae), Picrotoxinin (PTX, 10 μ M, n = 271,037 total ROIs in 9 larvae), or Melatonin (1 μ M, n = 350,516 total ROIs in 11 larvae).
C) Proportion of neurons belonging to each functional cluster across treatment groups. Distributions for violin plots are bootstrapped from 5000 replicates.
D) Same data as C, only showing the data for PTX vs DMSO vehicle control, re-ordered to reflect the cluster Adaptation Profiles grouped by cluster Response Shape.

Figure 6—figure supplement 1. Mean response of functionally identified clusters after different pharmacological treatments

253 the compounds were having the desired effects.

254 As PTX and Melatonin have opposing effects on habituation behaviour, we reasoned that these two treatments
255 should have opposite effects in the circuit, with PTX inhibiting depression and Melatonin promoting depression. In-
256 deed Melatonin has been found to increase the effects of GABA, and so such a relationship could be direct (*Cheng*
257 *et al.*, 2012; *Niles et al.*, 1987). In contrast to this straightforward hypothesis, what we observed was considerably
258 more complex. We did not observe alterations of the average response profiles of individual neuronal classes, which
259 remained indistinguishable after the treatments (*Figure 6-figure Supplement 1C-K*). Instead, the proportion of neu-
260 rons that belonged to the different classes was altered (*Figure 6B-D*). Therefore, the pharmacological manipulations
261 did not alter the activity of neurons in such a way as to alter the average activity states of populations, but instead
262 the proportion of neurons belonging to different populations changed. This may point to fixed and relatively inflexi-
263 ble processing strategies that the brain is using in the context of dark-flash habituation which constrain the possible
264 functional response types.

265 The effect of PTX on cluster reassignment generally tended towards weaker depression, increasing the propor-
266 tion of cells falling into the weaker depressing classes at the expense of strongly depressing classes for a given
267 response shape (*Figure 6D*). This pattern was most clear in the classes with “Short” and “Long” *Response Shapes*,
268 which are those that included the most strongly depressed classes of neurons.

269 Based on the hypothesis that Melatonin and GABA cooperate during habituation, we expected PTX and Mela-
270 tonin to have opposite effects. This clearly does not fit with our observations: for example, the size of the 12_M^{Pot}
271 neuron population was increased by both PTX and Melatonin (*Figure 5C*). While habituation of the Probability of
272 response is oppositely modulated by PTX and Melatonin, this is not true of behaviour globally – the behavioural
273 fingerprints of Melatonin and GABA are not opposites (*Figure 5A,B*) and opposing effects are not seen for the ha-
274 bituation of Displacement (*Figure 5-figure Supplement 1E,F*). Therefore, a lack of coherent shifts across the entire
275 neural population when applying these treatments is expected. However, opposite effects of PTX and Melatonin
276 were observed for 4_L^{strgD} neurons (*Figure 6C*), which we found to be most strongly correlated with motor output (*Fig-*
277 *ure 2F*), and thus is most closely associated with behavioural initiation. Therefore, this class might be most critical
278 for habituation of response Probability.

279 Combined, these experiments reveal that pharmacological manipulations that affect habituation behaviour man-
280 ifest in complex functional alterations in the circuit. These effects can not be captured by a simple model, and con-
281 siderable additional knowledge of the circuit, including the connectivity and signalling capacity of different neurons
282 will be necessary to understand these dynamics.

283 Identification of GABAergic neurons classes in the habituating circuit

284 Since our experiments point to the importance of GABAergic inhibition in habituation, we asked which functional
285 classes of neurons are GABAergic? An obvious model would assign a GABAergic identity to the 12_M^{Pot} neurons that
286 potentiate their responses, and thus could act to progressively depress the responses of other neuronal classes. We
287 began with virtual co-localization analyses with 3D atlases to identify candidate molecular markers for functionally
288 identified neurons. Such a strategy can be powerful to generate hypotheses from brain-wide imaging data, provided
289 sufficient stereotypy exists in the positioning of neurons, and the relevant marker exists in the atlas (*Dunn et al.*,
290 2016; *Randlett et al.*, 2015). Therefore, we analyzed the spatial correlations for markers contained in the Z-Brain
291 (*Randlett et al.*, 2015), Zebrafish Brain Browser (*Gupta et al.*, 2018; *Marquart et al.*, 2017; *Tabor et al.*, 2018), and
292 mapZebrain atlases (*Kunst et al.*, 2018; *Shainer et al.*, 2022). We identified markers showing the highest spatial
293 correlations with any of our functional clusters (corr. > 0.15, n=89 of 752 markers), and organized these hierarchically
294 (*Figure 7A*). GABAergic reporter lines based on the *gad1b* promoter were located in a region of the hierarchy showing
295 greatest spatial similarity with 10_S^{noA} and 11_S^{weakD} (*Figure 7B-E*). An enrichment along the medial tectum is common to
296 markers in this region of the hierarchy, where the highest density of GABAergic neurons within the tectum reside.

297 To confirm that 10_S^{noA} and 11_S^{weakD} classes are GABAergic, we imaged the response of neurons in *Tg(Gad1b:DsRed)*;
298 *Tg(elavl3:H2B-GCaMP6s)* double transgenic larvae, and classified neurons as *gad1b*-positive or -negative based on
299 DsRed/GCaMP levels (*Figure 7F,G*). Indeed we saw a heterogeneous distribution of *gad1b*-positive neurons across
300 functional clusters, including a significant enrichment in not only 10_S^{noA} and 11_S^{weakD} , but also the other two clusters
301 with the “Short” *Response Shape* (7_S^{medD} and 8_S^{strgD}). The remaining clusters either showed no significant bias, indicating

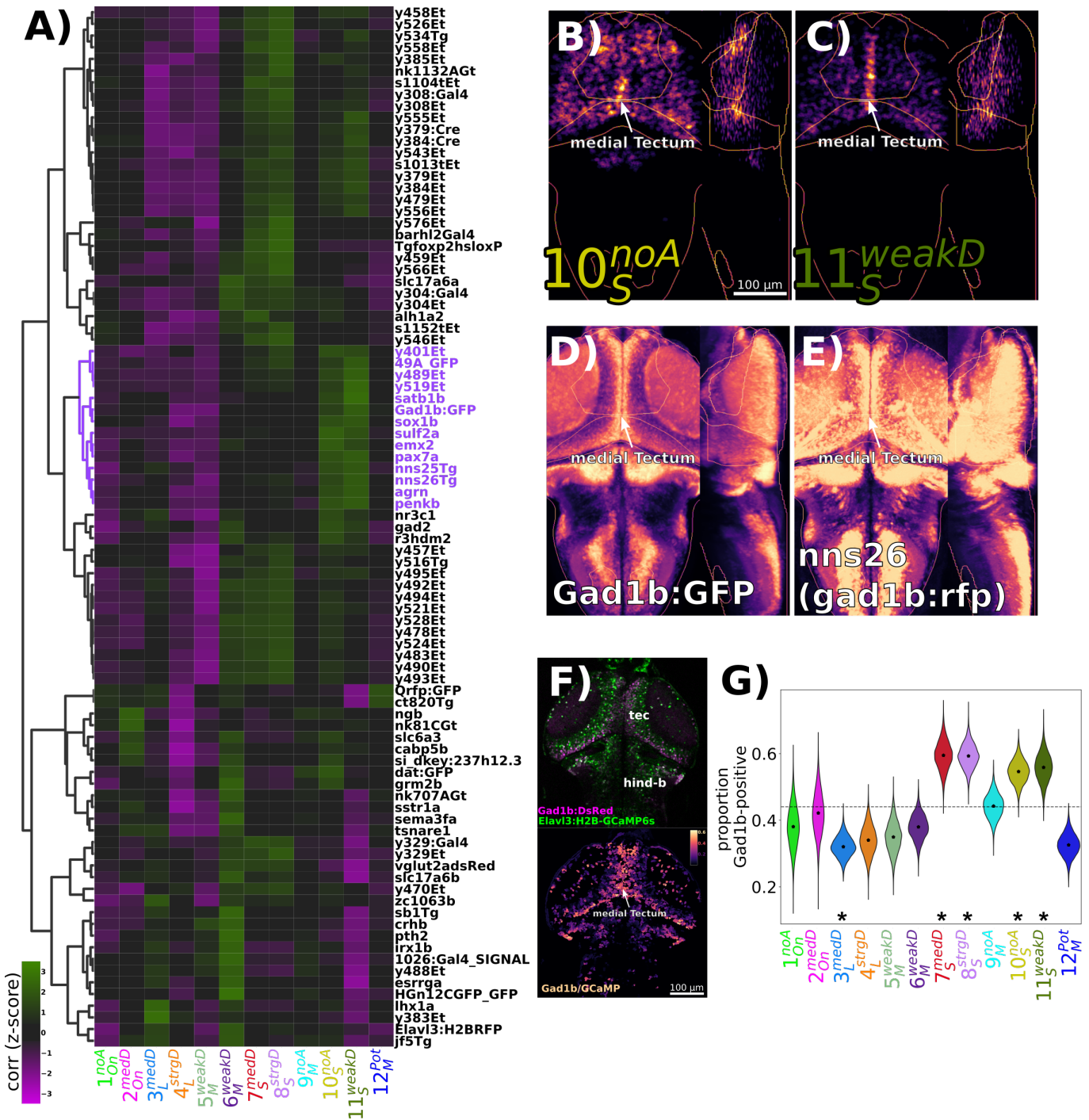


Figure 7. Identification of GABAergic neuronal classes

A) Hierarchically clustered heatmap depicting the correlation of markers aligned to the Z-Brain atlas with the spatial arrangement of the 12 functional clusters (distance = complete, correlation). Correlation values are z-scored by rows to highlight the cluster(s) most strongly correlated or anti-correlated with a given marker. The subset of the hierarchy containing the *gad1b*-reporters is coloured in purple.

B-D) Normalized summed intensity projections of **B)** 10^{noA} , and **C)** 11^{weakD} , **D)** *TgBAC(gad1b:GFP)* (*Satou et al., 2013*), Z-Brain Atlas, and **E)** *nns26*, aka *TgBAC(gad1b:LOXP-RFP-LOXP-GFP)* (*Satou et al., 2013*), mapZebrin Atlas

F) 2-photon imaging of *Tg(Gad1b:DsRed);Tg(elavl3:H2B-GCaMP6s)* larvae depicting the raw data for each channel (top), and the ratio of Gad1b/GCaMP6s fluorescence in each ROI functionally identified using suite2p.

G) ROIs imaged in double transgenic larvae are assigned a cluster identity based on their correlation to the cluster mean trace, and classified as Gad1b-positive based on a DsRed/GCaMP6s ratio of greater than 0.25. Dotted line = expected proportion based on total number of cells classified as Gad1b-positive. *= $p<0.05$, Chi Square test with Bonferroni correction. Distributions for violin plots calculated by bootstrapping 5000 replicates. $n = 1835$ ROIs in 6 larvae.

302 that they contain mixed populations, or a significant depletion of *gad1b*-positive cells, suggesting that they comprise
303 mostly of excitatory or neuromodulatory neurons (3_L^{medD} and 12_M^{Pot}).

304 These experiments indicate that GABAergic neurons in the habituating circuit are not characterized by their
305 *Adaptation Profile* (other than non-potentiating), and instead have a characteristic "Short" *Response Shape*, perhaps
306 reflecting a transient bursting style of activity relative to other neuronal types that exhibit more sustained firing
307 patterns. This lack of coherence in adaptation profile may explain why global manipulations of GABAergic signaling
308 through PTX have complex manifestations in the functional properties of neurons (Figure 6D)

309 Discussion

310 Molecular mechanisms of DF habituation

311 In the data resulting from our small molecule screen, we focused our analysis on those pharmacological agents
312 and pathways that strongly and relatively specifically modulated habituation when measuring response probability.
313 We found that inhibition of GABA_{A/C} Receptors using PTX reduced habituation learning. GABA is the main inhibitory
314 neurotransmitter in the zebrafish brain, and deficits in GABA signaling lead to epileptic phenotypes (Baraban et al.,
315 2005). We were fortunate that our screening concentration (10 μM) did not induce seizures, but was still sufficient to
316 inhibit habituation. This implies that the habituation circuit is exquisitely sensitive to changes in GABA signaling at
317 levels well below the threshold required to globally change excitatory-inhibitory balances. This argues for a central
318 rather than supporting role of GABAergic inhibition in dark-flash habituation.

319 A critical role for GABA in habituation is consistent with data from *Drosophila*, where both olfactory and gustatory
320 habituation have been linked to GABAergic interneurons (Das et al., 2011; Paranjpe et al., 2012; Trisal et al., 2022).
321 Therefore, this circuit motif of increasing inhibition to drive habituation may be a conserved feature of habituation,
322 which would allow for a straightforward mechanism for habituation override during dis-habituation via dis-inhibition
323 (Cooke and Ramaswami, 2020; Trisal et al., 2022).

324 Our screen also identified that neuro-hormonal signaling is critical for habituation, where Melatonin and Estro-
325 gen receptor agonists potently increase habituation learning rate. The role of Estrogens in learning and memory
326 is well established (Luine et al., 1998; Nilsson and Gustafsson, 2002). Though its role in habituation is less well ex-
327 plored, it has previously been shown to increase memory retention for olfactory habituation in mice (Dillon et al.,
328 2013). To our knowledge, Melatonin has not previously been implicated in habituation, though it has been impli-
329 cated in other learning paradigms (El-Sherif et al., 2003; Jilg et al., 2019). Notably, Melatonin was shown to block
330 operant learning at night in adult zebrafish (Rawashdeh et al., 2007), and therefore Melatonin appears to be able
331 to both promote or inhibit plasticity in zebrafish, depending on the paradigm.

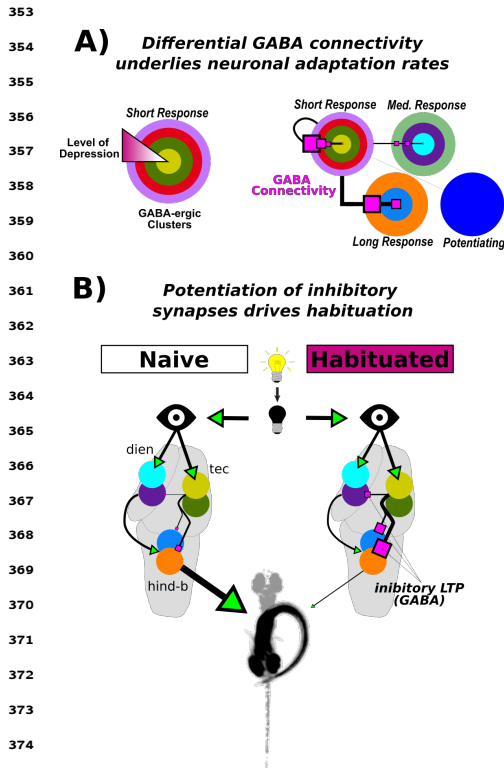
332 While Melatonin and Estrogen were not strong candidates for involvement in DF habituation plasticity before our
333 screen, their previous associations with learning and memory reinforce the idea that these molecules play critical
334 roles in plasticity processes. In support of this idea, we have previously shown that habituation is regulated in a
335 circadian-dependent manner (Randlett et al., 2019), and both Melatonin and Estrogen levels fluctuate across the
336 circadian cycle (Alvord et al., 2022; Gandhi et al., 2015; Zhdanova et al., 2001), suggesting that either or both of
337 these pathways may act to couple the circadian rhythm with learning performance.

338 Finally, approximately 2% of the US population use Melatonin as a sleep-aid (Li et al., 2022), and a substan-
339 tial proportion of US women take Estrogen as part of either oral contraceptives or hormone replacement therapy.
340 Therefore, understanding the roles these molecules play in neuroplasticity is a clear public health concern.

341 Circuit mechanisms of DF habituation

342 Based on behavioural experiments, we previously postulated that multiple plasticity loci cooperate in the habituat-
343 ing dark-flash circuit, arranged in both parallel and series within the circuit (Randlett et al., 2019). Here, our Ca²⁺
344 imaging experiments identified a diverse range of neuronal *Adaptation Profiles*, including non-adapting and potenti-
345 ating neurons spread throughout sensory- and motor- related areas of the brain. Thus, non-habituated signals are
346 transmitted throughout the brain, consistent with a distributed learning process. Such a model is further supported
347 with brain-wide imaging data for short-term habituation to looming stimuli, where distributed neurons were identi-
348 fied that showed differential rates of habituation (Marquez-Legorreta et al., 2022). It is important to point out that
349 Marquez-Legorreta et al. did not observe non-adapting or potentiating neurons in their experiments. This may be

350 due to differences in analysis methods, or could highlight a difference between short- and long-term habituation
 351 circuit mechanisms, the latter of which may rely on more complex circuit mechanisms involving both potentiation
 352 and suppression of responses.



376 **Figure 8.** Working models of dark flash habituation.
 377 **A)** Model proposed to explain how biased GABAergic
 378 inhibition may mediate the differential depression
 379 rates observed across neurons. Model proposes
 380 that the neurons with a short *Response Shape* are
 381 GABAergic, and that they differentially connect to
 382 the other functional subtypes, as well as themselves,
 383 to drive the response decreases observed during
 384 habituation. The strength of this inhibitory
 385 connectivity determines the decrease in
 386 responsiveness across neuronal classes. Larger pink
 387 box = Stronger inhibition. Cell types are depicted by
 388 the color scheme in **Figure 2**.
B) Proposed circuit model for the habituation of the
 389 probability of responding to a DF stimulus. The dark
 390 flash stimulus is detected by the retina and sent as
 391 an unadapted signal to the brain. GABAergic
 392 inhibitory neurons form the critical node in the
 393 habituating circuit, where habituation occurs as the
 394 result of a potentiation of GABAergic synapses,
 395 resulting in depressed responses in connected
 396 neurons. The strength of neuronal adaptation
 397 during habituation depends on the GABAergic
 398 connectivity strength (as in **B**). The output neurons
 399 of the circuit are the Long-responding class.
 400 Potentiated GABAergic inhibition onto this
 population silences behavioural output.

While we have insufficient anatomical data to constrain circuit connectivity models that drive DF habituation, here we demonstrate the use of pharmacology, functional imaging and neurotransmitter classifications to constrain our models. Specifically, pharmacology indicated a central role for GABA in habituation, and our functional imaging highlighted a role for distinct classes of neuronal types in the DF circuit, including potentiating neurons (12_{M}^{Pot}). These results point to a model where 12_{M}^{Pot} neurons are GABAergic and thus progressively inhibit the other neuronal classes. However, in silico co-localization analyses and double transgenic Ca^{2+} imaging identified 12_{M}^{Pot} neurons as predominantly non-GABAergic, inconsistent with this simple model. Instead, we found that the GABAergic neurons in the circuit are characterized by their short burst of activity to the stimulus onset. If the GABAergic neurons are not increasing in their firing rates but do drive habituation, then perhaps it is the potentiation of GABAergic synapses that drives habituation (**Figure 8**). This is a somewhat unexpected model, as studies of long-term synaptic plasticity (e.g. LTP and LTD) have overwhelmingly focused on plasticity at excitatory synapses. Although a functional link to behaviour is less well established, long-term inhibitory synaptic plasticity has been well documented, including inhibitory (i)-LTP and i-LTD (*Castillo et al., 2011*).

A key question then is what underlies the ranges in *Adaptation Profiles* that we see in individual neurons, which include non-adapting, weak-, medium-, and strong-depressing profiles. One possible model is that i-LTP is implemented differentially, which would require a mechanism to drive differential plasticity along different places in the circuit. While feasible, we favor a more parsimonious model in which differential connectivity from inhibitory neurons underlie these dynamics: non-adapting neurons receive little inhibition thus i-LTP has little effect, while strong-depressing neurons receive strong inhibitory connections undergoing i-LTP (**Figure 8A**). While this model is certainly incomplete, it provides the initial framework for the circuit-wide mechanisms leading to DF habituation, and testable hypotheses as to the connectivity and functional consequences of manipulations of different neuronal classes.

Conspicuously absent from our models are the 12_{M}^{Pot} neurons. Since these neurons were increased by both PTX and Melatonin, they might play a complex role in habituation. How they influence the system remains to be seen, but perhaps they act to reinforce activity in weakly habituating neurons. Given their location in the hindbrain they may alternatively directly feed into the reticulospinal system to modulate motor commands as the kinematics of the O-bend response change. Also absent from our current model are the classes exhibiting an On-response profile (1_{On}^{noA} and 2_{On}^{medD}). These neurons fire at the ramping off-

401 set of the stimulus, making it unlikely that they play a role in aspects of acute DF behaviour we measured here.
402 These neurons exist in both non-adapting and depressing forms suggesting a yet unidentified role in behavioural
403 adaptation to repeated DFs.

404 **Circuit loci of DF habituation**

405 Where in the brain does habituation take place? As discussed above and previously, our data is inconsistent with
406 a single-locus of plasticity (*Randlett et al., 2019*). Instead, we propose that plasticity is distributed throughout the
407 circuit. Since PTX inhibits most aspects of habituation learning (*Figure 5Ai*), these all may all involve GABAergic
408 motifs. Moreover, the different functional classes of neurons are distributed through sensory- and motor-related
409 areas of the brain, consistent with the notion that habituation plasticity occurs in a very distributed manner. While
410 distributed, there are clear associations between anatomical location and functional neuron type (*Figure 2A-E*), in-
411 dicating that there is some degree of regional logic to the localization of *Adaptation Profiles*. For example, 5_M^{weakD}
412 and 6_M^{weakD} are the most prevalent in the pretectum, and mostly absent from the tegmentum and posterior hind-
413 brain, whereas 3_L^{medD} and 4_L^{strgD} are numerous in tegmentum and posterior hindbrain, and thus likely occupy more
414 downstream positions in the sensori-motor circuit.

415 The tectum is one of the largest brain areas in larval zebrafish, and is directly innervated by nearly all retinal
416 ganglion cells (*Robles et al., 2014*). Therefore, the tectum is a prime candidate for implementing DF habituation for
417 anatomical reasons. In further support of this notion, the neurons we have identified as GABAergic and propose
418 to be driving habituation (7_S^{medD} , 8_S^{strgD} , 10_S^{noA} and 11_S^{weakD}) are concentrated in the tectum (*Figure 2C,D*). The tectum
419 contains multiple anatomically distinct types of GABAergic neurons, most of which are locally projecting interneu-
420 rons (SINs, ITNs, PVINs), although GABAergic projection neurons have been observed with axons projecting to the
421 anterior hindbrain (*Gebhardt et al., 2019; Martin et al., 2022; Nevin et al., 2010; Robles et al., 2011*). Therefore, we
422 expect that our GABAergic classes correspond to subsets of these GABAergic tectal neurons, which is testable using
423 genetic approaches based on marker co-expression and/or single cell morphometric and transcriptomic analyses.

424 Beyond the tectum, conspicuous neuronal clustering was observed in the inferior olive and cerebellum, which
425 have been implicated in motor-related learning behaviours in larval zebrafish (*Ahrens et al., 2012; Lin et al., 2020;*
426 *Markov et al., 2021*). Both structures contained many stimulus-tuned neurons (*Figure 1I*), and non-adapting (1_{On}^{noA} ,
427 9_M^{noA} and 10_S^{noA}), and potentiating (12_M^{pot}) neurons were among the most concentrated in the cerebellum (*Figure 2C,D*).
428 Non-adapting 9_M^{noA} neurons were also prominent in the torus longitudinalis, which also contains high concentrations
429 of on-responding 1_{On}^{noA} , 2_{On}^{medD} neurons. The torus longitudinalis has recently been implicated in the binocular integra-
430 tion of luminance cues (*Tesmer et al., 2022*), and therefore is ideally placed to influence habituation to whole-field
431 stimuli like DFs.

432 Collectively, our brain-wide imaging data point to a central role for inhibitory neurons in the tectum in habitua-
433 tion, but also clearly implicate other brain areas, and therefore a comprehensive model will need to span many
434 regions of the brain in order to explain the neural and behavioural dynamics underlying habituation learning.

435 **Conclusion**

436 Habituation is the simplest form of learning, yet despite its presumed simplicity a model of how this process is
437 regulated in the vertebrate brain is still emerging. Here we have combined two powerful methods offered by the
438 larval zebrafish model: whole brain functional imaging and high-throughput behavioural screening. By applying
439 these methods to long-term habituation, we identified dozens of pharmacological agents that strongly modulate
440 habituation learning and distinct classes of neurons that are activated by DFs and adapt their activity during learning.
441 The systematic datasets we generated contain large amounts of additional information that await future validation
442 and integration into a unified model for DF habituation. Nonetheless they yielded a multitude of hypotheses as to
443 the molecular and circuit mechanisms of habituation that can be followed up in future studies.

444 Our approach validates the utility of virtual anatomical analyses using atlases and pharmacological manipula-
445 tions to test and constrain neural circuit models in pan-neuronal imaging experiments, for which anatomical and
446 molecular information is often sparse. From these analyses we have arrived at the first iteration of a working model
447 for long-term dark flash habituation *Figure 8*. The diversity of molecular pathways and functional neuronal types
448 we have identified here indicate that considerable biological complexity exists that awaits discovery within the “sim-
449 plest” form of learning.

450 **Methods**

451 **Animals**

452 All experiments were performed on larval zebrafish at 5 days post fertilization (dpf), raised at a density of ≈ 1 larva/ml of E3 media in a 14:10h light/dark cycle at 28-29°C. Wild type zebrafish were of the TLF strain (ZDB-GENO-
453 990623-2). Transgenic larvae used were of the following genotypes: *Tg(elavl3:H2B-GCaMP7f)j^{f90}* (Yang et al., 2021),
454 *Tg(elavl3:H2B-GCaMP6s)j^{f5}* (Freeman et al., 2014), and *Tg(gad1b:DsRed)nns26* (Satou et al., 2013). Zebrafish were housed,
455 cared for, and bred at the Harvard MCB, UPenn CDB, and Lyon PRECI zebrafish facilities. All experiments were done
456 in accordance with relevant approval from local ethical committees at Harvard University, the University of Pennsylvania,
457 and the University of Lyon.

459 **High-throughput screening setup and protocol**

460 Larvae were assayed for behaviour in 300-well plates using the apparatus described previously (Randlett et al.,
461 2019). Briefly, each well is 8mm in diameter and 6mm deep, yielding a water volume of $\approx 300\mu\text{L}$. Behaviour plates
462 are suspended below a water bath kept at 31°C, which acts as a heated lid to prevent condensation and maintains
463 the water temperature in the well at 29°C. Behaviour was tracked using a Mikrotron CXP-4 camera, Bitflow CTN-
464 CX4 frame grabber, illuminated with IR LEDs (TSHF5410, digikey.com). Visual stimuli were delivered via a ring of 155
465 WS2812B RGB LEDs (144LED/M, aliexpress.com). For a dark flash stimulus, the LEDs were turned off for 1s, and then
466 the light intensity was increased linearly to the original brightness over 20s. The optomotor response was induced
467 by illuminating every 8th LED along the top and bottom of the plate, and progressively shifting the illuminated
468 LED down the strip resulting in an approximately sinusoidal stimulus, 5.5 cm peak to peak, translating at 5.5 cm
469 per second. Direction of motion was switched every 30 s, for a total testing period of 1 hour, and performance was
470 scored as the average change in heading direction towards the direction of motion during these 30s epochs. Acoustic
471 tap stimuli were delivered using a Solenoid (ROB-10391, Sparkfun). The behavioural paradigm was designed to be
472 symmetrical such that 1hr worth of stimulation was followed by 1hr worth of rest (Figure 1B), allowing us to alternate
473 the view of the camera between two plates using 45-degree incidence hot mirrors (43-958, Edmund Optics) mounted
474 on stepper motors (Figure 1A, ROB-09238, Sparkfun), driven by an EasyDriver (ROB-12779, Sparkfun).

475 Apparatus were controlled using arduino microcontrollers (Teensy 2.0 and 3.2, PJRC) interfaced with custom
476 written software (Multi-Fish-Tracker), available here:

477 github.com/haesemeyer/MultiTracker.

478 The protocol for assessing behaviour (Figure 1B, Figure 3B) consisted of dark flashes repeated at 1-minute inter-
479 vals, delivered in 4 training blocks of 60 stimuli, separated by 1hr of rest (from 0:00-8:00, hr:min of the protocol). For
480 analyses, this epoch is separated into periods reflective of the Naive response (first 5 stimuli), and the remaining 235
481 stimuli during training. From 8:00-8:30, no stimuli are delivered and fish are monitored for spontaneous behaviour.
482 From 8:30-9:00 fish are given acoustic stimuli, and from 10:00 - 11:00 fish are assayed for the optomotor response
483 and turning towards the direction of motion (light blue). Finally, at 12:00-13:00, larvae are given 60 additional dark
484 flashes during the test period (red).

485 **Behavioural analyses**

486 The behaviour of the fish was tracked online at 28 hz, and 1-second long videos at 560 hz were recorded in response
487 to DF and Acoustic Tap stimuli. Offline tracking on recorded videos was performed in MATLAB (Mathworks) using the
488 script "TrackMultiTrackerTiffStacks_ParallelOnFrames.m", as described previously, to track larval posture (Randlett
489 et al., 2019). Tracks were then analyzed using Python. Analysis code available here:
490 github.com/owenrandlett/lamire_2022.

491 Responses to DFs and to taps were identified as movement events that had a bend amplitude greater than 3rad
492 and 1rad , respectively. Behavioural fingerprints were created by first calculating the average value for each fish
493 reflecting either the DF response during the specified time period (Naive = DFs 1-5, Training = DFs 6-240, Test = DFs
494 241-300), or the average response during the entire stimulus period (Acoustic Taps, OMR, Free Swimming). Periods
495 where the tracking data was incomplete were excluded from the analysis. DFs where larvae did not respond were
496 excluded from the behavioural components other than the Probability of Response. The Strictly Standardized Mean
497 Difference was then calculated for each of these average fish values for the compound-treated larvae relative to the

498 vehicle (DMSO) control (*Figure 3C*). The threshold for determining hit compounds was set at $|SSMD| \geq 2$. These
499 analyses were performed using:

500 [Analyze_MultiTracker_TwoMeasures.py](#).

501 Hierarchical clustering (*Figure 3D*, *Figure 4A-C*) was performed using SciPy (*Virtanen et al., 2020*). Correlations
502 across different behavioural measures (*Figure 4B*) was calculated computing all pairwise comparisons for each be-
503 havioural measure in the SSMD fingerprint across the 176 hit compounds.

504 Further details and code for the analyses used to create the figure panels are in the following notebook:
505 [2022_LamireEtAl_BehavFigs.ipynb](#). Analyses made use of open-source Python packages, including: NumPy (*Harris*
506 *et al., 2020*), SciPy (*Virtanen et al., 2020*), matplotlib (*Hunter, 2007*), seaborn (*Waskom, 2021*), and open-cv (*Bradski,*
507 *2000*).

508 **Pharmacology**

509 Compounds were prepared as 1000x frozen stock solutions in DMSO. Stock solutions were initially diluted 1:100 in
510 E3, yielding a 10x solution. 30uL of this solution was then pipetted into the wells, yielding a 1x compound solution
511 in 0.1% DMSO (Sigma). Vehicle treatment followed the same protocol, using pure DMSO. Larvae were incubated in
512 compound solution for between 30 to 90 minutes prior to behavioural testing.

513 The small molecule compound library (Selleckchem Bioactive: FDA-approved/FDA-like small molecules, *Figure 1-*
514 *source data 1*) was obtained from the UPenn High-Throughput Screening Core. The library concentration was
515 10mM, and thus all compounds were screened at approximately 10uM. For subsequent pharmacological exper-
516 iments chemicals were obtained from: Picrotoxinin: Sigma, P-8390; Melatonin: Cayman, 14427; Sigma, M5250;
517 Ethinyl Estradiol: Cayman, 10006486; Hexestrol: Sigma, H7753

518 **Microscopy**

519 Imaging was performed on 5dpf larvae, mounted tail-free in 2% LMP agarose (Sigma A9414) in E3, using a 20x
520 1.0NA water dipping objective (Olympus). Volumetric Imaging (*Figure 1*,*Figure 2*, *Figure 6*) was performed at 930
521 nm on a Bruker Ultima microscope at the CIQLE imaging platform (Lyon, LYMIC), using a resonant scanner resonant
522 scanner over a rectangular region of 1024x512 pixels (0.6 μ m x/y resolution) and piezo objective mount for fast z-
523 scanning. Imaging sessions began by taking an "Anatomy Stack" consisting of 150 slices at 1 μ m z-steps, summed
524 over 128 repeats (imaging time \approx 11 minutes). This served as the reference stack used for alignment to the Z-Brain
525 atlas, and to detect Z-drift in the imaging session (see below). The functional stack consisted of 12 slices separated at
526 10 μ m steps, thus covering 120 μ m in the brain acquired at 1.98 hz. To image *Tg(elavl3:H2B-GCaMP6s);Tg(gad1b:DsRed)*
527 double transgenic larvae (*Figure 7*), we used a custom built 2-photon microscope (*Haesemeyer et al., 2018*), imaging
528 512x512 images at (0.98 μ m x/y resolution) at 1.05 hz. The anatomy stack was taken at 2 μ m step sizes for both the
529 green and red channels in the dark. Functional imaging was performed only on the green/GCaMP channel since the
530 red stimulus LED was incompatible with DsRed imaging.

531 When developing this protocol we determined that substantial shifts of more than a cell-body diameter (5 μ M) in
532 the Z-plane are common during the \approx 1.2 hrs of imaging. We determined this by comparing the sum of the functional
533 image planes during 5 equally sized time epochs (1540 frames per epoch), aligned to the "Anatomy Stack", using
534 "phase_cross_correlation" in the scikit-image library (*van der Walt et al., 2014*). This allowed us to quantify shifts
535 in the imaging plane as shifts in this alignment. These tended to occur within the first hour of imaging, therefore
536 we performed an hour of imaging of this functional stack before beginning the DF stimulation protocol to allow the
537 preparation to settle under imaging conditions. Dark flashes were delivered using a 3mm red LED mounted above
538 the fish, controlled by an Arduino Nano connected to the microscope GPIO board and the Prairie View software to
539 deliver pulses of darkness consisting of 1 sec light off, 20 sec linear ramp back to light on, delivered at 60 second
540 intervals.

541 Even with this pre-imaging protocol, z-shifts were still observed in a considerable number of fish. Since our
542 habituation-based analysis is focused on how individual neurons change their responses over time, shifts in the
543 z-plane are extremely problematic as they are not correctable post-acquisition and can result in different neurons
544 being imaged at individual voxels. This could easily be confused for changes in functional responses over time during
545 habituation. Therefore, any fish showing a z-drift of greater than 3 μ m was excluded from our analysis. Stable z-
546 positioning was further confirmed by manual inspection of the eigen images in the imaging timecourse using "View

547 registration metrics" in suite2 to confirm that these do not reflect z-drift. Of 56 larvae imaged total, 22 were
548 excluded, leaving 34 included. Larvae were treated with 0.1% DMSO, Picrotoxinin (PTX, 10uM), or Melatonin (1uM),
549 from approximately 1hr before imaging. These fish were analyzed as a single population (*Figure 1*,*Figure 2*) and
550 separately to determine the effects of the treatments (*Figure 6*).

551 **Ca²⁺ imaging analysis**

552 ROIs were identified using suite2p (*Pachitariu et al., 2017*) using the parameters outlined in
553 *RunSuite2p_BrukerData_ScreenPaper.py* and *RunSuite2p_MartinPhotonData_ScreenPaper.py* scripts for the data
554 from the Bruker Ultima microscope (*Figure 5*-*Figure 8*), and custom built 2-photon microscope (*Figure 7D,E*), respec-
555 tively. These ROIs mostly reflected individual neuronal nuclei/soma. The imaging planes were then aligned to the
556 anatomical stack taken before functional imaging using "phase_cross_correlation" in the scikit-image library (*van der*
557 *Walt et al., 2014*). For the volumetric data, the anatomical stack was then aligned to the Z-Brain atlas coordinates
558 using CMTK, and ROI coordinates were transformed into Z-Brain coordinates using streamxform in CMTK. These
559 steps were performed using *Bruker2p_AnalyzePlanesAndRegister.py*.

560 To identify ROIs that were correlated with the stimulus we use a regression-based approach (*Miri et al., 2011*),
561 where we identified ROIs that were correlated with vectors representing the time course of the DF stimuli convolved
562 with a kernel approximating the slowed H2B-GCaMP time course with respect to neuronal activity. These regressors
563 reflected either the entire 21 second dark flash stimulus, or only the onset of the flash, and either the first 3, last 3,
564 or all 60 flashes (6 regressors in total). To identify neurons correlated to motor output, we took advantage of the
565 plane-based registration statistics calculated by suite2p. Specifically, the "ops['corrXY']" metric, which reflects the
566 correlation of each registered image frame with the reference image. We reasoned that movements would cause
567 image artifacts and distortions that would be reflected as a transient drop in these correlations. Indeed, we con-
568 firmed this association by imaging the tail using an infrared camera, and compared the motion index calculated
569 through tail tracking, and that which we calculated based on the motion artifacts, which showed good overall agree-
570 ment in predicted movement events and average correlation of 0.4, demonstrating that these image-based artifacts
571 can be used as reliable proxies of tail movements (*Figure 1*-*figure Supplement 1*). Therefore, regressors based on
572 these motion indices were used to identify neurons correlated with motor output.

573 Images for the functional tuning of individual neurons (*Figure 1G-J*) were computed using the the Hue Saturation
574 Value (HSV) colorscheme, with the maximal correlation value to either regressor mapped to saturation, and the
575 hue value reflecting the linear preference for either regressor. Clustering of functional response types (*Figure 2*)
576 was done by first selecting all those ROIs that showed a correlation of 0.25 or greater with any of the 6 stimulus
577 regressors across all imaged fish. Then among these ROIs we removed any ROIs that did not show a correlation of
578 0.3 or greater with at least 5 ROIs imaged in a different larvae. This filtered out ROIs that were unique in any individual
579 fish, allowing us to focus on those neuron types that were most consistent across individuals. We then used the
580 Affinity Propagation clustering from scikit-learn (*Pedregosa et al., 2011*), with "affinity" computed as the Pearson
581 product-moment correlation coefficients (corrcoef in NumPy (*Harris et al., 2020*)), preference=-9, and damping=0.9.

582 To generate the final cluster assignments we re-scanned all the ROIs calculating their correlation with the mean-
583 response vectors for each of the identified 12 functional clusters, selecting those with a correlation value of 0.3 or
584 greater, which were then assigned to the cluster with which they had the highest correlation. To determine the clus-
585 ter assignments for the data from *Tg(Gad1b:DsRed);Tg(elavl3:H2B-GCaMP6s)* double transgenic larvae (*Figure 7F,G*)
586 data were realigned and interpolated to match the frame rate of the clustered data, and assigned to the 12 clusters
587 as above.

588 To compare the spatial relationships between the neuronal positions of different functional clusters (*Figure 2E*),
589 and between the functional clusters and reference brain labels (*Figure 7A-E*), image volumes were cropped to the
590 imaged coordinates (*Figure 1E*), downsampled to isometric 10 um³ voxels, and linearized to calculate the Pearson's
591 correlation coefficient between the image sub-volumes.

592 Analyses made use of multiple open-source Python packages, including: suite2p (*Pachitariu et al., 2017*) NumPy
593 (*Harris et al., 2020*), SciPy (*Virtanen et al., 2020*), scikit-learn (*Pedregosa et al., 2011*), scikit-image (*van der Walt et al.,*
594 *2014*), numba (*Lam et al., 2015*), matplotlib (*Hunter, 2007*), seaborn (*Waskom, 2021*), and open-cv (*Bradski, 2000*).

595 Details of the analyses used to create the figure panels are in the following notebook:

596 *2022_LamireEtAl_FunctionalFigs.ipynb*

597 Data and Code Availability

598 Code for data analysis and for generating the figure panels is available here:
599 github.com/owenrandlett/lamire_2022
600 Data are available here:
601 lamire2022.randlettlab.com/

602 Acknowledgments

603 We thank the Randlett, Granato and Engert group members for helpful advice regarding the manuscript and work,
604 Gregory Forkin for help in zebrafish husbandry, the Burgess and Baier groups for sharing anatomical data from
605 the Zebrafish Brain Browser and mapZebrain atlases, and Armin Bahl for sharing the mapZebrain to Z-Brain trans-
606 formation. This work was supported by funding from the ATIP-Avenir program of the CNRS and Inserm (O.R.), a
607 Fondation Fyssen research grant (O.R.), the IDEX-Impulsion initiative of the University of Lyon (O.R.), the NIH grants
608 MH109498 (M.G.), NS123887 (M.H.), U19NS104653 and 1R01NS124017 (F.E.), the National Science Foundation grant
609 IIS- 1912293 (F.E.), and the Simons Foundation grant SCGB 542973 (F.E.)

610 Author Contributions

611 Conceptualization: OR, MG
612 Methodology: OR
613 Software: OR, MH
614 Formal Analysis: OR
615 Investigation: L-AL, OR
616 Supervision, Resources and Funding Acquisition: FE, MG, OR
617 Writing – Original Draft Preparation: OR
618 Writing – Review & Editing: MH, FE, MG, LA-L, OR
619

620 References

- 621 Ahrens MB, Li JM, Orger MB, Robson DN, Schier AF, Engert F, Portugues R. Brain-wide neuronal dynamics during motor adaptation
622 in zebrafish. *Nature*. 2012 May; 485(7399):471–477.
- 623 Alvord VM, Kantra EJ, Pendergast JS. Estrogens and the circadian system. *Semin Cell Dev Biol*. 2022 Jun; 126:56–65.
- 624 Bailey CH, Chen M. Morphological basis of long-term habituation and sensitization in Aplysia. *Science*. 1983 Apr; 220(4592):91–93.
- 625 Bandara SB, Carty DR, Singh V, Harvey DJ, Vasylieva N, Pressly B, Wulff H, Lein PJ. Susceptibility of larval zebrafish to the seizurogenic
626 activity of GABA type A receptor antagonists. *Neurotoxicology*. 2020 Jan; 76:220–234.
- 627 Baraban SC, Taylor MR, Castro PA, Baier H. Pentylenetetrazole induced changes in zebrafish behavior, neural activity and c-fos
628 expression. *Neuroscience*. 2005; 131(3):759–768.
- 629 Bradski G. The openCV library. *Dr Dobb's Journal: Software Tools for the Professional Programmer*. 2000; 25(11):120–123.
- 630 Bruni G, Rennekamp AJ, Velenich A, McCarroll M, Gendelev L, Fertsch E, Taylor J, Lakhani P, Lensen D, Evron T, Lorello PJ, Huang
631 XP, Kolczewski S, Carey G, Caldarone BJ, Prinsen E, Roth BL, Keiser MJ, Peterson RT, Kokel D. Zebrafish behavioral profiling
632 identifies multitarget antipsychotic-like compounds. *Nat Chem Biol*. 2016 Jul; 12(7):559–566.
- 633 Burgess HA, Granato M. Modulation of locomotor activity in larval zebrafish during light adaptation. *J Exp Biol*. 2007 Jul; 210(Pt
634 14):2526–2539.
- 635 Castillo PE, Chiu CQ, Carroll RC. Long-term plasticity at inhibitory synapses. *Curr Opin Neurobiol*. 2011 Apr; 21(2):328–338.
- 636 Chen X, Engert F. Navigational strategies underlying phototaxis in larval zebrafish. *Front Syst Neurosci*. 2014 Mar; 8:39.
- 637 Cheng XP, Sun H, Ye ZY, Zhou JN. Melatonin modulates the GABAergic response in cultured rat hippocampal neurons. *J Pharmacol
638 Sci*. 2012 May; 119(2):177–185.

- 639 Cooke SF, Komorowski RW, Kaplan ES, Gavornik JP, Bear MF. Visual recognition memory, manifested as long-term habituation,
640 requires synaptic plasticity in V1. *Nat Neurosci*. 2015 Feb; 18(2):262–271.
- 641 Cooke S, Ramaswami M. Ignoring the Innocuous: The Neural Mechanisms of Habituation. In: *The Cognitive Neurosciences: 6th
642 Edition* MIT Press; 2020.p. 197.
- 643 Das S, Sadanandappa MK, Dervan A, Larkin A, Lee JA, Sudhakaran IP, Priya R, Heidari R, Holohan EE, Pimentel A, Gandhi A, Ito K,
644 Sanyal S, Wang JW, Rodrigues V, Ramaswami M. Plasticity of local GABAergic interneurons drives olfactory habituation. *Proc
645 Natl Acad Sci U S A*. 2011 Sep; 108(36):E646–54.
- 646 Dillon TS, Samuel Dillon T, Fox LC, Han C, Linster C, 17β -estradiol enhances memory duration in the main olfactory bulb in CD-1
mice; 2013.
- 648 Dunn TW, Mu Y, Narayan S, Randlett O, Naumann EA, Yang CT, Schier AF, Freeman J, Engert F, Ahrens MB. Brain-wide mapping of
649 neural activity controlling zebrafish exploratory locomotion. *Elife*. 2016 Mar; 5:e12741.
- 650 El-Sherif Y, Tesoriero J, Hogan MV, Wierszko A. Melatonin regulates neuronal plasticity in the hippocampus. *J Neurosci Res*. 2003;
651 72(4):454–460.
- 652 Förster D, Helmbrecht TO, Mearns DS, Jordan L, Mokayes N, Baier H, Retinotectal circuitry of larval zebrafish is adapted to detection
653 and pursuit of prey; 2020.
- 654 Freeman J, Vladimirov N, Kawashima T, Mu Y, Sofroniew NJ, Bennett DV, Rosen J, Yang CT, Looger LL, Ahrens MB. Mapping brain
655 activity at scale with cluster computing. *Nat Methods*. 2014 Sep; 11(9):941–950.
- 656 Gandhi AV, Mosser EA, Oikonomou G, Prober DA. Melatonin is required for the circadian regulation of sleep. *Neuron*. 2015 Mar;
657 85(6):1193–1199.
- 658 Gebhardt C, Auer TO, Henriques PM, Rajan G, Duroure K, Bianco IH, Del Bene F. An interhemispheric neural circuit allowing
659 binocular integration in the optic tectum. *Nat Commun*. 2019 Nov; 10(1):5471.
- 660 Glanzman DL. Habituation in Aplysia: the Cheshire cat of neurobiology. *Neurobiol Learn Mem*. 2009 Sep; 92(2):147–154.
- 661 Gupta T, Marquart GD, Horstick EJ, Tabor KM, Pajevic S, Burgess HA. Morphometric analysis and neuroanatomical mapping of the
662 zebrafish brain. *Methods*. 2018 Nov; 150:49–62.
- 663 Haesemeyer M, Robson DN, Li JM, Schier AF, Engert F. A Brain-wide Circuit Model of Heat-Evoked Swimming Behavior in Larval
664 Zebrafish. *Neuron*. 2018 May; 98(4):817–831.e6.
- 665 Harris CR, Millman KJ, van der Walt SJ, Gommers R, Virtanen P, Cournapeau D, Wieser E, Taylor J, Berg S, Smith NJ, Kern R, Picus M,
666 Hoyer S, van Kerkwijk MH, Brett M, Haldane A, Del Río JF, Wiebe M, Peterson P, Gérard-Marchant P, et al. Array programming
667 with NumPy. *Nature*. 2020 Sep; 585(7825):357–362.
- 668 Hayden DJ, Montgomery DP, Cooke SF, Bear MF. Visual recognition is heralded by shifts in local field potential oscillations and
669 inhibitory networks in primary visual cortex. *J Neurosci*. 2021 Jun; 41(29):6257–6272.
- 670 Hunter JD. Matplotlib: A 2D graphics environment. *Computing in Science & Engineering*. 2007; 9(3):90–95. doi:
671 [10.1109/MCSE.2007.55](https://doi.org/10.1109/MCSE.2007.55).
- 672 Jilg A, Bechstein P, Saade A, Dick M, Li TX, Tosini G, Rami A, Zemmar A, Stehle JH. Melatonin modulates daytime-dependent synaptic
673 plasticity and learning efficiency. *J Pineal Res*. 2019 Apr; 66(3):e12553.
- 674 Kaplan ES, Cooke SF, Komorowski RW, Chubykin AA, Thomazeau A, Khibnik LA, Gavornik JP, Bear MF. Contrasting roles for
675 parvalbumin-expressing inhibitory neurons in two forms of adult visual cortical plasticity. *Elife*. 2016 Mar; 5.
- 676 Kunst M, Laurell E, Mokayes N, Kramer A, Kubo F, Fernandes AM, Förster D, Dal Maschio M, Baier H. A Cellular-Resolution Atlas
677 of the Larval Zebrafish Brain; 2018.
- 678 Lam SK, Pitrou A, Seibert S. Numba: a LLVM-based Python JIT compiler. In: *Proceedings of the Second Workshop on the LLVM Compiler
679 Infrastructure in HPC* No. Article 7 in LLVM '15, New York, NY, USA: Association for Computing Machinery; 2015. p. 1–6.
- 680 Li J, Somers VK, Xu H, Lopez-Jimenez F, Covassin N. Trends in Use of Melatonin Supplements Among US Adults, 1999–2018. *JAMA*.
681 2022 Feb; 327(5):483–485.
- 682 Lin Q, Manley J, Helmreich M, Schlumm F, Li JM, Robson DN, Engert F, Schier A, Nöbauer T, Vaziri A. Cerebellar Neurodynamics
683 Predict Decision Timing and Outcome on the Single-Trial Level. *Cell*. 2020 Jan; 0(0).

- 684 **Luine VN**, Richards ST, Wu VY, Beck KD. Estradiol enhances learning and memory in a spatial memory task and effects levels of
685 monoaminergic neurotransmitters. *Horm Behav.* 1998 Oct; 34(2):149–162.
- 686 **Markov DA**, Petrucco L, Kist AM, Portugues R. A cerebellar internal model calibrates a feedback controller involved in sensorimotor
687 control. *Nat Commun.* 2021 Nov; 12(1):6694.
- 688 **Marquart GD**, Tabor KM, Horstick EJ, Brown M, Geoca AK, Polys NF, Nogare DD, Burgess HA. High-precision registration between
689 zebrafish brain atlases using symmetric diffeomorphic normalization. *Gigascience.* 2017 Aug; 6(8):1–15.
- 690 **Marquez-Legorreta E**, Constantin L, Piber M, Favre-Bulle IA, Taylor MA, Blevins AS, Giacometto J, Bassett DS, Vanwalleghem GC,
691 Scott EK. Brain-wide visual habituation networks in wild type and fmr1 zebrafish. *Nat Commun.* 2022; 13(1):1–19.
- 692 **Martin A**, Babbitt A, Pickens AG, Pickett BE, Hill JT, Suli A. Single-Cell RNA Sequencing Characterizes the Molecular Heterogeneity
693 of the Larval Zebrafish Optic Tectum. *Front Mol Neurosci.* 2022 Feb; 15:818007.
- 694 **McDiarmid TA**, Belmadani M, Liang J, Meili F, Mathews EA, Mullen GP, Hendi A, Wong WR, Rand JB, Mizumoto K, Haas K, Pavlidis P,
695 Rankin CH. Systematic phenomics analysis of autism-associated genes reveals parallel networks underlying reversible impairments
696 in habituation. *Proc Natl Acad Sci U S A.* 2019 Nov; .
- 697 **McDiarmid TA**, Yu AJ, Rankin CH. Habituation Is More Than Learning to Ignore: Multiple Mechanisms Serve to Facilitate Shifts in
698 Behavioral Strategy. *Bioessays.* 2019 Aug; 8:1900077.
- 699 **Miri A**, Daie K, Burdine RD, Aksay E, Tank DW. Regression-based identification of behavior-encoding neurons during large-scale
700 optical imaging of neural activity at cellular resolution. *J Neurophysiol.* 2011 Feb; 105(2):964–980.
- 701 **Nelson JC**, Shoenhard HM, Granato M. Pharmacogenetic and whole-brain activity analyses uncover integration of distinct molec-
702 ular and circuit programs that drive learning; 2022.
- 703 **Nevin LM**, Robles E, Baier H, Scott EK, Focusing on optic tectum circuitry through the lens of genetics; 2010.
- 704 **Niles LP**, Pickering DS, Arciszewski MA. Effects of chronic melatonin administration on GABA and diazepam binding in rat brain. *J
705 Neural Transm.* 1987; 70(1-2):117–124.
- 706 **Nilsson S**, Gustafsson JA. Biological role of estrogen and estrogen receptors. *Crit Rev Biochem Mol Biol.* 2002; 37(1):1–28.
- 707 **Pachitariu M**, Stringer C, Dipoppa M, Schröder S, Rossi LF, Dalgleish H, Carandini M, Harris KD. Suite2p: beyond 10,000 neurons
708 with standard two-photon microscopy; 2017.
- 709 **Paranjpe P**, Rodrigues V, VijayRaghavan K, Ramaswami M. Gustatory habituation in Drosophila relies on rutabaga (adenylate
710 cyclase)-dependent plasticity of GABAergic inhibitory neurons. *Learn Mem.* 2012 Nov; 19(12):627–635.
- 711 **Pedregosa F**, Varoquaux G, Gramfort A, Michel V, Thirion B, Grisel O, Blondel M, Prettenhofer P, Weiss R, Dubourg V, Others.
712 Scikit-learn: Machine learning in Python. *the Journal of machine Learning research.* 2011; 12:2825–2830.
- 713 **Ramaswami M**. Network Plasticity in Adaptive Filtering and Behavioral Habituation. *Neuron.* 2014 Jun; 82(6):1216–1229.
- 714 **Randlett O**, Haesemeyer M, Forkin G, Shoenhard H, Schier AF, Engert F, Granato M. Distributed Plasticity Drives Visual Habituation
715 Learning in Larval Zebrafish. *Curr Biol.* 2019 Apr; 29(8):1337–1345.e4.
- 716 **Randlett O**, Wee CL, Naumann EA, Nnaemeka O, Schoppik D, Fitzgerald JE, Portugues R, Lacoste AMB, Riegler C, Engert F, Schier
717 AF. Whole-brain activity mapping onto a zebrafish brain atlas. *Nat Methods.* 2015 Sep; 12(11):1039–1046.
- 718 **Rankin CH**, Abrams T, Barry RJ, Bhatnagar S, Clayton DF, Colombo J, Coppola G, Geyer MA, Glanzman DL, Marsland S, McSweeney
719 FK, Wilson DA, Wu CF, Thompson RF. Habituation revisited: an updated and revised description of the behavioral characteristics
720 of habituation. *Neurobiol Learn Mem.* 2009 Sep; 92(2):135–138.
- 721 **Rawashdeh O**, de Borsetti NH, Roman G, Cahill GM. Melatonin suppresses nighttime memory formation in zebrafish. *Science.*
722 2007 Nov; 318(5853):1144–1146.
- 723 **Rihel J**, Prober DA, Arvanites A, Lam K, Zimmerman S, Jang S, Haggarty SJ, Kokel D, Rubin LL, Peterson RT, Schier AF. Zebrafish
724 behavioral profiling links drugs to biological targets and rest/wake regulation. *Science.* 2010 Jan; 327(5963):348–351.
- 725 **Robles E**, Laurell E, Baier H. The retinal projectome reveals brain-area-specific visual representations generated by ganglion cell
726 diversity. *Curr Biol.* 2014 Sep; 24(18):2085–2096.
- 727 **Robles E**, Smith SJ, Baier H. Characterization of genetically targeted neuron types in the zebrafish optic tectum. *Front Neural
728 Circuits.* 2011 Feb; 5:1.

- 729 **Rose JK**, Kaun KR, Chen SH, Rankin CH. GLR-1, a non-NMDA glutamate receptor homolog, is critical for long-term memory in
730 *Caenorhabditis elegans*. *J Neurosci*. 2003 Oct; 23(29):9595–9599.
- 731 **Satou C**, Kimura Y, Hirata H, Suster ML, Kawakami K, Higashijima SI. Transgenic tools to characterize neuronal properties of
732 discrete populations of zebrafish neurons. *Development*. 2013 Sep; 140(18):3927–3931.
- 733 **Shainer I**, Kuehn E, Laurell E, Al Kassar M, Mokayes N, Sherman S, Larsch J, Kunst M, Baier H. A single-cell resolution gene expression
734 atlas of the larval zebrafish brain; 2022.
- 735 **Tabor KM**, Marquart GD, Hurt C, Smith TS, Geoca AK, Bhandiwad AA, Subedi A, Sinclair JL, Polys NF, Burgess HA. Brain-wide cellular
736 resolution imaging of Cre transgenic zebrafish lines for functional circuit-mapping; 2018.
- 737 **Tesmer AL**, Fields NP, Robles E. Input from torus longitudinalis drives binocularity and spatial summation in zebrafish optic tectum.
738 *BMC Biol*. 2022 Jan; 20(1):24.
- 739 **Trisal S**, Aranha M, Chodankar A, VijayRaghavan K, Ramaswami M. A DROSOPHILA CIRCUIT FOR HABITUATION OVERRIDE. *J
740 Neurosci*. 2022 Mar; .
- 741 **Virtanen P**, Gommers R, Oliphant TE, Haberland M, Reddy T, Cournapeau D, Burovski E, Peterson P, Weckesser W, Bright J, van der
742 Walt SJ, Brett M, Wilson J, Millman KJ, Mayorov N, Nelson ARJ, Jones E, Kern R, Larson E, Carey CJ, et al. SciPy 1.0: fundamental
743 algorithms for scientific computing in Python. *Nat Methods*. 2020 Mar; 17(3):261–272.
- 744 **van der Walt S**, Schönberger JL, Nunez-Iglesias J, Boulogne F, Warner JD, Yager N, Gouillart E, Yu T, scikit-image contributors.
745 scikit-image: image processing in Python. *PeerJ*. 2014 Jun; 2:e453.
- 746 **Waskom M**. seaborn: statistical data visualization. *J Open Source Softw*. 2021 Apr; 6(60):3021.
- 747 **Yang E**, Zwart MF, Rubinov M, James B, Wei Z, Narayan S, Vladimirov N, Mensh BD, Fitzgerald JE, Ahrens MB. A brainstem integrator
748 for self-localization and positional homeostasis; 2021.
- 749 **Zhdanova IV**, Wang SY, Leclair OU, Danilova NP. Melatonin promotes sleep-like state in zebrafish. *Brain Res*. 2001 Jun; 903(1–
750 2):263–268.

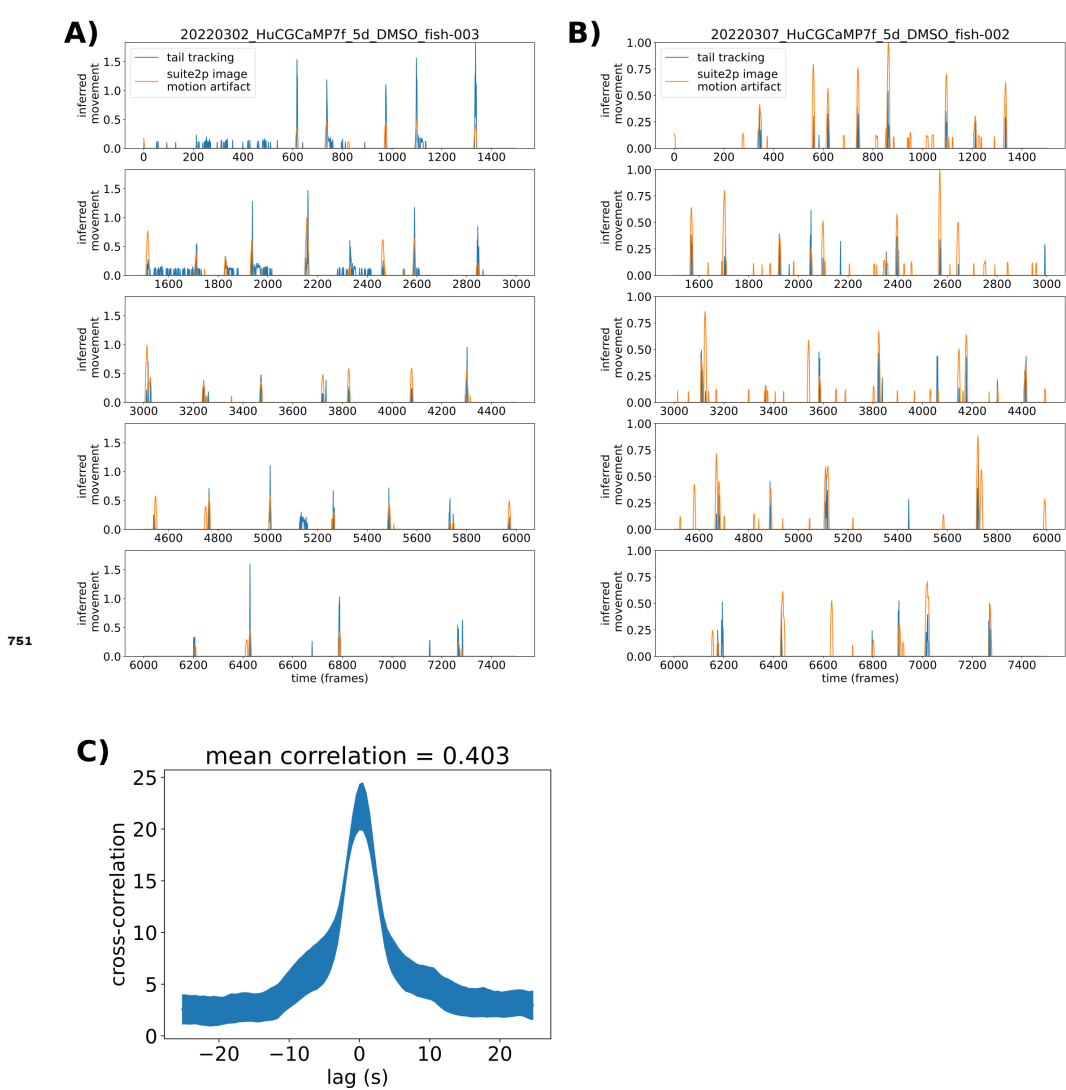


Figure 1—figure supplement 1. Validation of motion analysis based on image artifacts during 2-photon imaging.
A) Motion indexes as calculated based on tail tracking (blue) and based on decreases in the correlation between individual frames and the reference frame used for motion alignment (orange) across the entire imaging experiment (65 minutes).
B) Same analysis as (A), for a different larva.
C) Cross-correlation plot comparing the two motion index vectors. Mean across 6 larvae, and line thickness = standard error.

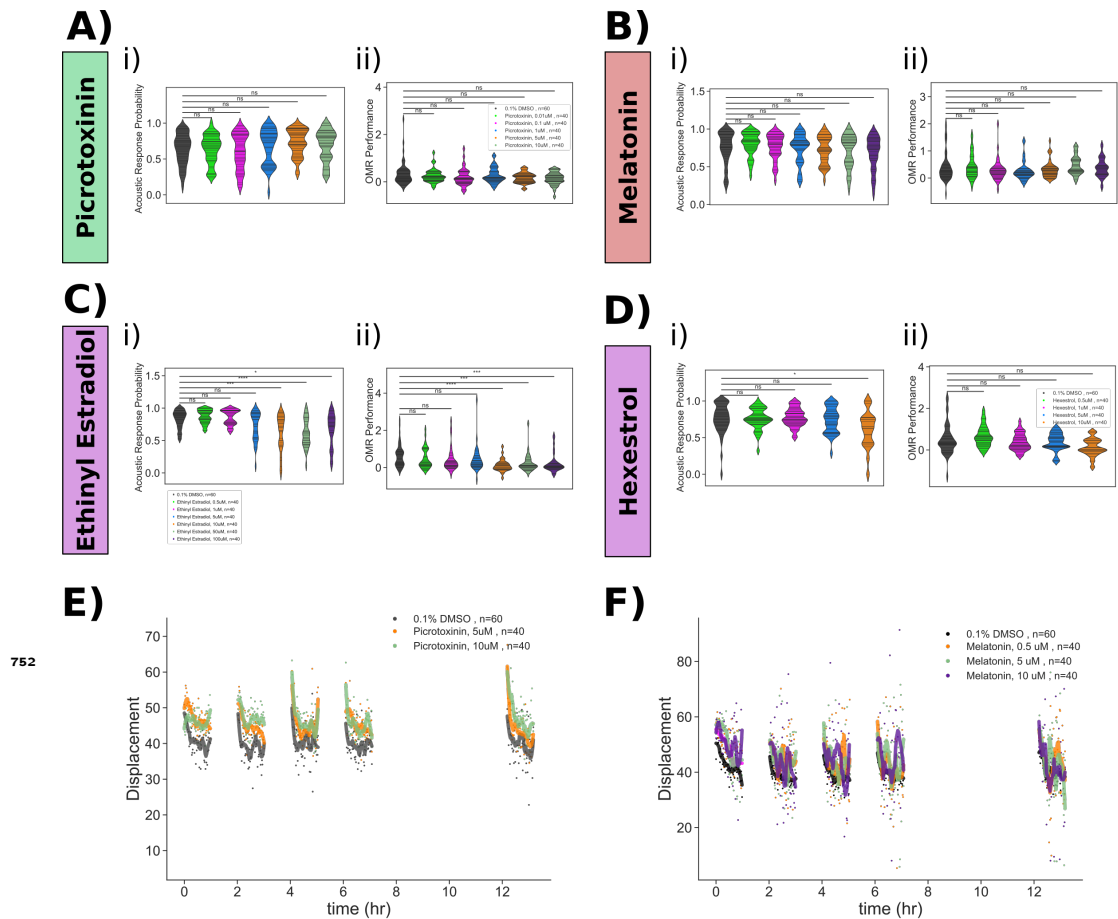


Figure 5—figure supplement 1. Pharmacological manipulation of control behaviours and response displacement during habituation.

Dose response studies for **A) Picrotoxinin**, **B) Melatonin**, **C) Ethynodiol Estradiol** and **D) Hexestrol**. Displayed for each treatment are: i) Violin plots for the dose response data, showing the probability of response to 30 acoustic tap stimuli. Horizontal lines = individual fish. ii) Violin plots for the dose response data OMR performance. Horizontal lines = individual fish. Statistical tests: Mann Whitney with bonferroni correction, ns=not significant; $p \leq **** = 1 \times 10^{-4}$; *** = 1×10^{-3} ; ** = 1×10^{-2} ; * = 0.05.

E) Treatment with Picrotoxinin inhibits the decreases in movement displacement during habituation training.

F) Treatment with Melatonin inhibits the decreases in movement displacement during habituation training. Each dot is the mean response of the population to one flash. Lines are smoothed in time with a Savgolay Filter (window = 15 stimuli, order=2).

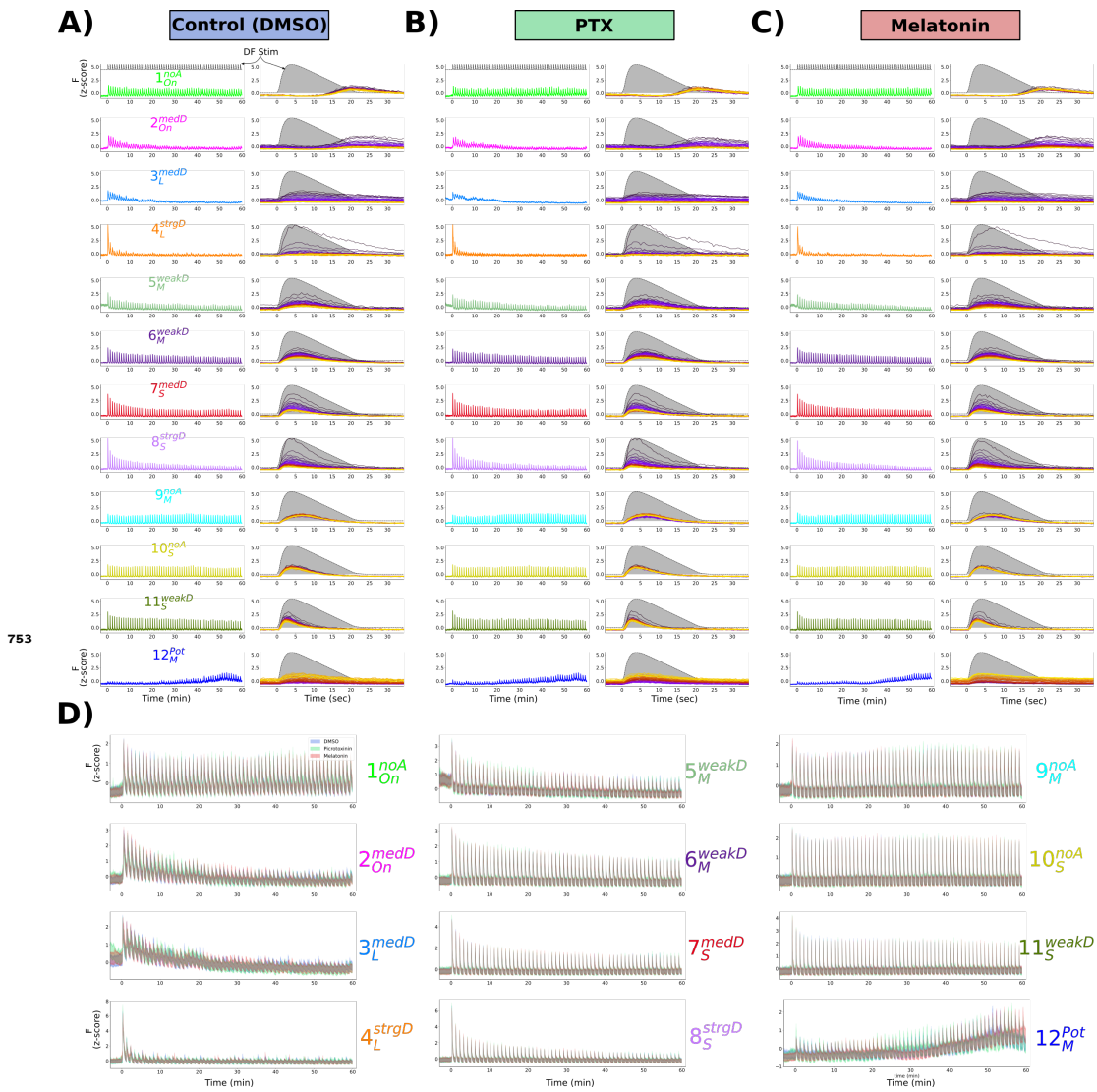


Figure 6—figure supplement 1. Mean response of functionally identified clusters after different pharmacological treatments. **A-C)** Average z-scored fluorescence each functional cluster plotted for the whole experiment (left column), and centered on each DF stimulus (right column), demonstrating the differences in both adaptation and *Response Shape* for each cluster after treatment with **(A)** 0.1% DMSO vehicle control, **(B)** Picrotoxinin (10 μ M), or **(C)** Melatonin (1 μ M). **D)** Same data as A-C, plotted together for each treatment group.